Robotica (2022), **40**, pp. 1538–1569
doi:10.1017/S0263574721001259

CAMBRIDGE
UNIVERSITY PRESS

RESEARCH ARTICLE

Enumeration and instantaneous mobility analysis of a class of 3-UPU parallel manipulators with equilateral triangular platforms

Sercan Boztaş and Gökhan Kiper*

Department of Mechanical Engineering, İzmir Institute of Technology, 35430 İzmir, Turkey
*Corresponding author. E-mail: gokhankiper@iyte.edu.tr.

Received: 17 April 2021; **Revised:** 14 June 2021; **Accepted:** 6 August 2021; **First published online:** 4 October 2021

Keywords: Parallel manipulators; enumeration; instantaneous mobility analysis

Abstract

In this study, several joint axis orientations on equilateral platforms and the limbs of 3-UPU parallel manipulators (PMs) are examined. The generated joint layouts for the platforms were matched with each other to generate and enumerate manipulator architectures based on certain assumptions. The structures of thus obtained manipulators are examined and limb types were determined. These limb types were analyzed using screw theory. The instantaneous mobility of the manipulators and the motion characteristics of the moving platforms are tabulated. The finite mobility analysis of one of the manipulators is performed using a software package as an example. Among several different 3-UPU PM architectures, 118 novel 3-UPU PMs with non-parasitic 3-degrees-of-freedom are significantly important. The classified 3-UPU PMs with determined motion characteristics can be used by researchers as a design alternative for their specific design task.

1. Introduction

Via topological design of joint locations and structures, it is possible to obtain generalizations of certain parallel manipulators (PMs) and to generate new architectures with different platform motion characteristics. As an example, Gao et al. [1] investigated generalizations of Stewart–Gough platforms by considering all possible geometric constraints (distance constraints) between six pairs of geometric primitives (points, lines or planes) on the base and the platform. Later, Toz and Kucuk [2,3] presented dimensional optimization of some asymmetric generalized Stewart–Gough platforms using particle swarm optimization.

In recent years, several lower mobility PMs have been developed. One of the commonly used lower mobility PM is the 3-UPU PM which was introduced for the first time by Tsai [4]. A 3-UPU PM consists of a fixed base platform and a moving platform connected by three limbs, each of which comprises Universal (U)—Prismatic (P)—Universal (U) joints in sequence. Typically, the U joints are passive and the P joints are actuated. Several different 3-UPU PM architectures can be obtained by altering the U joint axis arrangements on the base and/or moving platform. Many such different architectures have been presented and analyzed in terms of mobility, kinematic, singularity, dynamics, stiffness, workspace and positioning errors in the literature. 3-UPU PMs generically have 3-degrees-of-freedom (DoF) with pure translation, pure rotation or mixed motion of the moving platform. The type of the motion depends on the relative directions of universal joint axes on the limbs. Also, some 3-UPU PMs have different DoF in different assembly modes.

Mr. Sercan Boztaş is currently at Research and Development Department, Dirinler Machinery Industry Co, 35620 İzmir, Turkey

© The Author(s) 2021. Published by Cambridge University Press.

https://doi.org/10.1017/S0263574721001259 Published online by Cambridge University Press

The first 3-UPU PM presented by Tsai PM generically has three DoF and is designed for pure translational motion, that is, it is a translational PM (TPM). Mobility, kinematic, singularity, dynamic, stiffness, workspace, accuracy analyses and certain applications of the Tsai 3-UPU PM were issued by several researchers. These studies are summarized in Table I. The proposed application for the Tsai PM include machining [5], a walking robot for disabled people [6] and a functional magnetic resonance imaging (fMRI) device for examining the functioning of the human brain [7,8].

A 3-UPU PM with a different kind of joint layout, later on called the Seoul National University (SNU) PM, was introduced at the beginning of the new millennium. When mobility analysis of the SNU PM is theoretically computed, it is seen that the PM has three translational DoF. However, when the physical model of the PM was constructed, it was observed that the PM moved even when all the actuators are locked. Even the kinematic singularity analysis of the PM has not solved this problem. Later, researchers tried to explain this phenomenon by analyzing the kinematic sensitivity of the PM [9]. Wolf and Shoham [10], Liu et al. [11], Walter et al. [12], Gogu [13] and Qu et al. [14] have worked on the singularity analysis of the SNU PM. Bonev and Zlatanov [15], Wolf et al. [16], Zlatanov et al. [17], Li and Huang [18], Chen et al. [19] have also worked on the mobility analysis in addition to the singularity analysis. Kinematic analysis of the PM was studied by Li and Huang [18], Wolf and Shoham [20], Walter et al. [12] and Chen et al. [21].

Karouia and Hervé [48] designed a 3-UPU PM with a rotational platform for which necessarily the revolute (R) joint axes associated with the base and the moving platform intersect at a single point at all times of the motion of the PM. They worked on the mobility analysis of this spherical 3-UPU PM, whereas Di Gregorio [49] worked on the mobility, kinematic and singularity analyses of the PM. The singularity analysis of the PM was also studied by Di Gregorio [50] and Paganelli [51], while Chebbi et al. [52] and Pramanik and Ghosal [53] worked on kinematic and singularity analysis of the PM. Xiangzhou et al. [54,55] worked on the kinematics and dynamics of the PM. Pramanik and Ghosal [53] offered a solar tracking system using the spherical 3-UPU PM. Ashith Shyam and Ghosal [56] worked on path planning of this PM.

Huang and Li [57] designed 3-UPU PMs with the first U joint axes of the base or moving platform as perpendicular to the platform planes. The first analysis shows that this new type of PM generically has 4-DoF with three translational and one rotational DoF. Kiper and Söylemez [58] showed that when the base and the moving platform of the PM are identical, the PM has 4-DoF and furthermore, it has a finite singularity mode with 5-DoF when the limb lengths are the same. Guo et al. [59] investigated the position and orientation errors of the PM.

Huang et al. [60] presented a new type of 3-UPU TPM which is in the form of a pyramid. Yu et al. [61] proposed a 3-UPU PM architecture in which the R joint axes of the U joints of the base or moving platform are positioned parallel to each other inside the platform planes. Binbin et al. [62] studied the singularities of these PMs. Miao et al. [63] developed a rolling mechanism using such a 3-UPU PM, where the mobility, gait and stability analyzes of the PM were done. Zhao et al. [64] proposed a new PM with SNU 3-UPU-type U joints on the base, and vertical-type U joints on the moving platform. This PM possesses one translational and two rotational DoF. Lu and Hu [65] presented a new type of 3-UPU PM with an asymmetrical joint set-up, that is, the three U joints on a platform do not have same type of joint configuration. Lu et al. [66] presented PMs with SNU-type and vertical-type U joints. Hu and Lu [67] presented a stiffness analysis of one of these new type of PMs. Chebbi and Parenti-Castelli [68] presented a study with various types of 3-UPU PMs, where the singularities of the PMs were studied and their potentials were interpreted. Wang et al. [69–72] designed a robotic leg for 3-DoF translational motion using a 3-UPU PM. Sarabandi et al. [73] worked on an asymmetric 3-UPU PM which can be reconfigured to work either as a translational or a rotational PM by flipping upside down its moving platform. Zhao et al. [74] presented a novel 3-UPU PM with two rotational and one translational DOF without any parasitic motion. Di Gregorio [75] has recently presented a comprehensive review study on 3-UPU PMs and worked out motion characteristics of the PMs with special emphasis on TPMs and spherical PMs.

https://doi.org/10.1017/S0263574721001259 Published online by Cambridge University Press

https://doi.org/10.1017/S0263574721001259 Published online by Cambridge University Press

Table I. *Studies on the Tsai 3-UPU PM*

Author(s)	Mobility analysis	Kinematic analysis	Singularity analysis	Stiffness analysis	Workspace analysis	Error analysis	Application
Tsai [4]	+	+					
Tsai and Joshi [22]		+			+		
Tsai and Joshi [23]				+	+		
Joshi and Tsai [24]; Parenti-Castelli et al. [25]; Kanaan et al. [26,27]; Yang and O'Brien [28]			+				
Joshi and Tsai [29]		+		+	+		
Di Gregorio and Parenti-Castelli [30]; Zhao et al. [31]	+						
Di Gregorio and Parenti-Castelli [32]; Walter and Husty [33]; Yang and O'Brien [34]; Bałchanowski [35]		+	+				
Guan et al. [36]; Zhao et al. [37]	+		+				
Badescu and Mavroidis [38]					+		
Yi							Machining
Chebbi et al. [39]					+	+	
Qi et al. [6]	+				+		Walking robot for disabled people
Li et al. [7]	+			+	+		fMRI device for human brain
Dehkordi et al. [8]					+		fMRI device for human brain
Bi and Wen [40]						+	
Wang et al. [41]		+				+	
Sun [42]; Bhutani and Dwarakanath [43]		+					
Guohua et al. [44]				+	+		
Aboulissane and El Bakkali [45]	+	+	+		+		
Laribi et al. [46]; Wei et al. [47]		+			+		

This study aims to classify new 3-UPU PM architectures with typical U joint layouts, examine the instantaneous mobility characteristics of 3-UPU PMs with equilateral platforms and classify PMs with non-parasitic and parasitic motion patterns. To the best knowledge of the authors, such a classification of 3-UPU PM architectures is performed for the first time. In Section 2, PMs with the same kinematic structure as the 3-UPU PM were investigated and the properties of the PMs were introduced. In Section 3, joint layouts were created for 3-UPU PMs, and these joint layouts were mapped to each other to obtain new manipulators. When these obtained PMs were examined, it was observed that they had common limb types. In Section 4, these limb types were investigated by using screw theory. In Section 5, novel PMs are analyzed.

2. 3-UPU PM types according to joint layouts

3-UPU PMs presented in the literature were investigated and the joint layouts of the R joint axes on the platforms are examined. Based on the joint layouts of these 3-UPU PMs, new 3-UPU PM architectures are constructed.

2.1. Joint layouts of Tsai, SNU, parallel and vertical 3-UPU PMs

The R joint axes on the platforms of Tsai 3-UPU PM are coplanar, they form a triangle and are tangent to the circumcircle of the triangle formed by the U joint centers (Fig. 1(a)). For this reason, this kind of joint layout of the platform is denoted as U^T, where T stands for tangent. The three U joint centers on the base platform define the base platform plane, whereas the three U joint centers on the moving platform define the moving platform plane. The global coordinate system (GCS) is positioned at the center of the circumcircle of the U joint centers of the base of the PM. X-axis of the GCS is oriented towards one of the U joint centers on a limb. Y-axis of the GCS lies on the base platform plane whereas the Z-axis is perpendicular to the plane. The limb which comprises the U joint center on the X-axis is numerated as limb 1 and the other two limbs are numerated as limb 2 and limb 3 by proceeding in counter-clockwise direction about the Z-axis. Three local coordinate systems (LCS) for each limb are positioned at the U joint centers of the base. The axes of LCS1 are set to be parallel to the axes of the GCS. The axis orientations of LCS2 and LCS3 differ according to the 3-UPU architecture. For the Tsai 3-UPU PM, LCS2 and LCS3 are obtained by rotating LCS1 around the Z-axis by 120° and 240°, respectively. In other words, for the Tsai 3-UPU PM, the x-axes of the LCSs are normal and the y-axes are tangent to the circumcircle. The first and second R joint axes of a U joint on the base are the first joint axis (R_{i1}) and second joint axis (R_{i2}) of each limb i (i = 1, 2, 3). A P joint is the third joint of each limb, and the next two R joint axes of the U joint on the moving platform are called the fourth joint axis (R_{i4}) and the fifth joint axis (R_{i5}) of each limb. For the Tsai 3-UPU PM, R_{i1} are positioned on the y-axis of the LCSs and R_{i2} rotate about the y-axis and hence lie on the xz-plane of the LCSs. R_{i2} and R_{i4} are parallel axes. The joint layout of the moving platform is the same as the base platform, that is, R_{i5} are tangent to the circumcircle on the moving platform plane. Hence the Tsai 3-UPU PM architecture is denoted as U^T-U^T.

For the SNU 3-UPU PM, the R axes (R_{i1} or R_{i5}) on a platform (base or moving) lie on the platform plane and intersect in the circumcircle center of the triangle formed by the U-joint centers and hence are normal to the circumcircle (Fig. 1(b)). This kind of joint layout of the platform is denoted as U^N, where N stands for normal. R_{i1} of the SNU 3-UPU PM are positioned on the x-axis of the LCSs. The base and moving platforms have the same joint layout. R_{i2} and R_{i4} are parallel axes. The SNU 3-UPU PM architecture is denoted as U^N-U^N.

When the first axes on a platform lie on the platform plane and are all parallel to the X- or Y-axis of the GCS, the joint layout of the platform is denoted as U^X or U^Y. The LCS axes of all three limbs are parallel to the axes of the GCS axes as shown in Fig. 1(c). Depending on which R joint axes are attached to the platforms, the architecture of the PM in Fig. 1(c) may be U^X-U^X or U^Y-U^Y or U^X-U^Y or U^Y-U^X. R_{i2} and R_{i4} are either parallel or perpendicular to each other.

https://doi.org/10.1017/S0263574721001259 Published online by Cambridge University Press

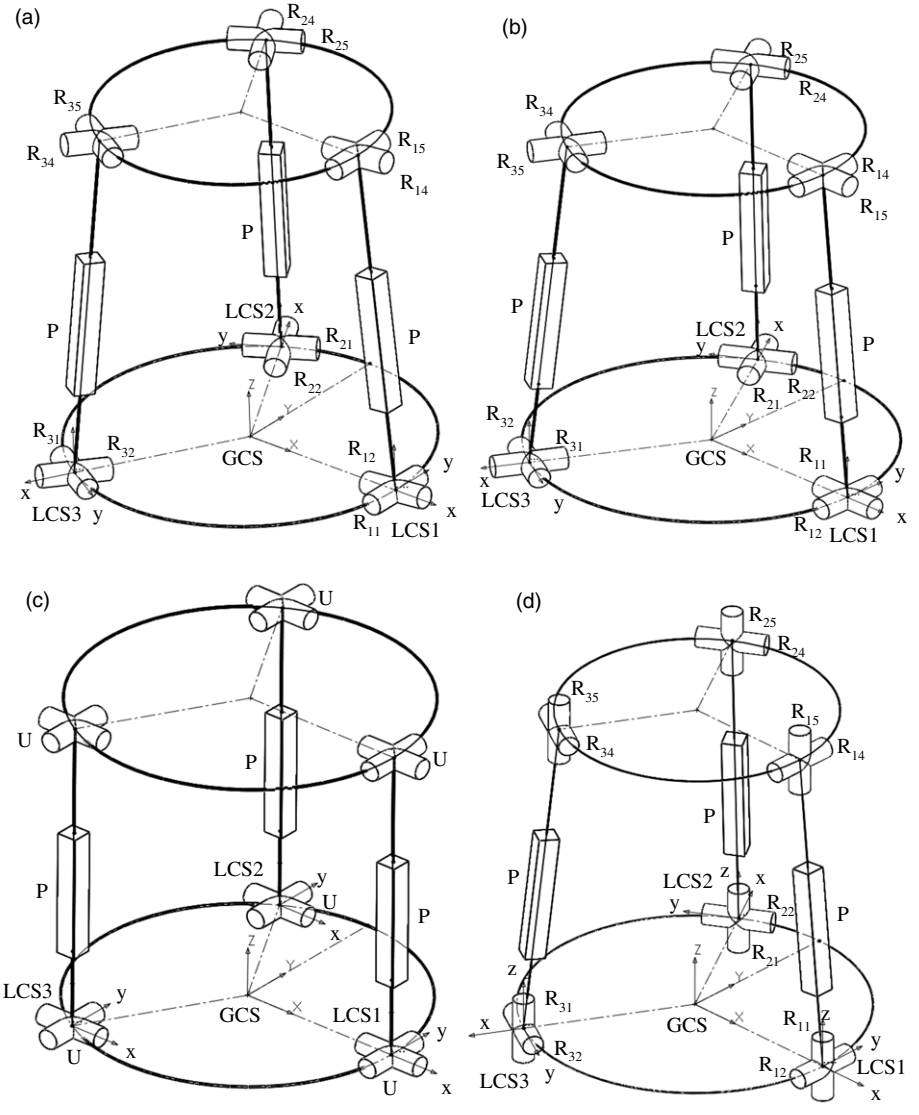


Figure 1. *Joint layouts of (a) Tsai 3-UPU PM, (b) SNU 3-UPU PM, (c) Parallel 3-UPU PM, (d) Vertical 3-UPU PM.*

When the first R axes on a platform are perpendicular to the platform plane, the joint layout of the platform is denoted as U^{V}. There are several possibilities for the relative positions of the R_{i2} and R_{i4} axes. In order to distinguish between different R_{i2} and R_{i4} axes configurations, an initial configuration of the PM is considered. For the PMs comprising platforms with U^{V} type, the initial configuration of the PM, according to the orientation of the second axes the U joint (R_{i2} or R_{i4}) may be denoted as U^{VT}, U^{VN}, U^{VX} or U^{VY}. The locations of the LCSs for Vertical 3-UPU PM is the same as the Tsai 3-UPU PM. R_{i1} are positioned on the z-axes of the LCSs. For U^{VT}, R_{i2} are on the y-axes (Fig. 1(d)). For U^{VN}, R_{i2} are on the x-axes of the LCSs. For U^{VX} and U^{VY}, R_{i2} is on either x- or y-axes of the LCSs.

2.2. Sub-joint layouts for 3-UPU PMs

In general, a U-joint mounted on a platform can have ∞^2 possible configurations, which depends on the orientation of the R joint axis attached to the platform. So, in general for a platform comprising three

https://doi.org/10.1017/S0263574721001259 Published online by Cambridge University Press

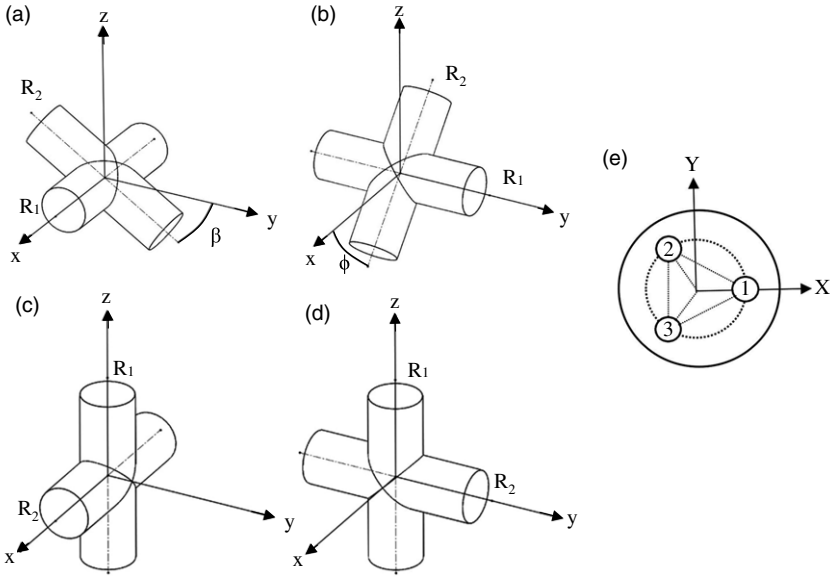


Figure 2. *R joint axes of a U joint when R_{i1} are on (a) x-axis, (b) y-axis, (c, d) z-axis of the LCS (e) U-joint layout representation of a platform.*

U-joints, there are ∞^6 possible joint layouts. Also, the relative locations of R_{i2} and R_{i4} axes on each limb should be considered for a 3-UPU PM. This can be taken into account by defining the R_{i2} and R_{i4} axes in an initial configuration, which is specifying the angle between R_{i2} and R_{i4}. Therefore, in general, there are ∞^{15} possible 3-UPU architectures. Among these abundantly many possible architectures, not all are practical. Therefore, based on the available architectures in the literature, some ground rules are established in order to narrow down the list to a reasonable finitely many possible architectures.

In the literature, it is seen that generally the distances between the U-joint centers of a platform are taken to be equivalent, that is, base and moving platforms are in equilateral triangle form. Therefore, in this study, only the 3-UPU PMs with equilateral base and moving platforms are considered. However, the base and the moving platforms need not be identical. In order to be able to perform the mobility analysis of different 3-UPU PM architectures, an initial configuration is set such that the moving platform plane is parallel to the base platform plane, the center of the moving platform is on the Z-axis of the GCS and all three limbs make a prescribed angle with the base platform plane. The relative positions of the joint axes are then defined based on this initial configuration.

Due to the particular shape of the U joint, it is known that the position of the R_{i2} and R_{i4} axes can be predicted by looking at the R_{i1} and R_{i5} axes of the U joints. As shown in Fig. 2(a), if R_{i1} axis of a U joint is along the x-axis of a LCS, R_{i2} axis must move on the yz-plane. Similarly, if R_{i1} axis is along the y-axis (Fig. 2(b)), R_{i2} axis must move on the xz-plane. Similar arguments are valid for R_{i5} and R_{i4} axes of the moving platform as well.

R_{i2} and R_{i4} axes have to be nonintersecting, that is, parallel or skew, because of the P joint in between them. The P joint direction cannot be in the direction of the R_{i2} or R_{i4} axes, otherwise a cylindrical joint is obtained. The P joint direction has to be perpendicular to R_{i2} and R_{i4} axes. Furthermore, it is assumed that the common normal of R_{i2} and R_{i4} axes pass through the two U-joint centers on limb i. With these assumptions, the orientations of R_{i2} and R_{i4} axes in the initial configuration of the PM are determined depending on the angle between the limbs and the platform planes. If R_{i1} or R_{i5} axes are perpendicular to the base or moving platform planes, that is, if R_{i1} axes are on the z-axis of the corresponding LCSs, R_{i2} and R_{i4} have to be on the platform planes, but the relative positions of R_{i2} and R_{i4} axes cannot be predicted. So, in such a case, the orientation of the R_{i2} and R_{i4} axes in the initial configuration should be specified (Fig. 2(c) and (d)).

https://doi.org/10.1017/S0263574721001259 Published online by Cambridge University Press

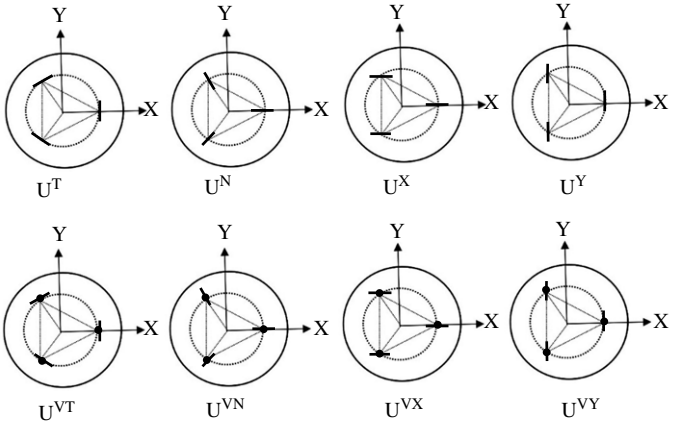


Figure 3. *R-joint layouts of a platform.*

The case where R_{i1} and R_{i5} axes are neither on nor perpendicular to the platform planes is kept out of scope of this study. To sum up the previous discussions, when R_{i1} or R_{i5} axes are on the platform plane, the orientations of R_{i2} and R_{i4} axes are determined according to the angle between the limbs and the platforms in the initial configuration of the PM, while when R_{i1} or R_{i5} axes are perpendicular to the platform plane, the orientations of R_{i2} and R_{i4} axes in the initial configuration of the PM need to be specified. By this way, it is possible to provide a proper description of the PM architecture that enables to derive new U joint layouts. As seen in Fig. 2(e), the U joints are numbered in the same order as the LCSs.

When R_{i1} or R_{i5} axes are on a platform plane, it is assumed that either of the following four cases occur: (1) the axes are tangent to the circle passing through the U-joint centers on a platform (U^T); (2) the axes are normal to the circle passing through the U-joint centers on a platform (U^N); (3) the axes are all parallel to the X-axis of the GCS (U^X); (4) the axes are all parallel to the Y-axis of the GCS (U^Y). When R_{i1} or R_{i5} axes are perpendicular to a platform plane, the layout is shown with U^{VT}, U^{VN}, U^{VX} or U^{VY}, depending on whether the R_{i2} or R_{i4} axes are tangent, normal or parallel to X- or Y-axis, respectively. Graphical representation of all these possible U-joint layouts is illustrated in Fig. 3.

On a platform, it is also possible to have U-joint layouts where, for example two of the R_{i1} axes are tangent to the platform circle, while the remaining R_{i1} axis is normal. Such new layouts are obtained by changing the type of one of the three U-joints on a platform. The changed U-joint is assumed to be on limb 1. The case, where all three U-joints are from different layouts are kept out of scope of this study. In order to represent the created subgroups, the main layout associated with the two U-joints is written as a superscript, while the U-joint to be modified is written as a subscript. For example, U^T_N for a base platform represents a joint layout where the R_{11} axis is normal, while R_{21} and R_{31} are tangent to the circle passing through the U-joint centers. Different layouts for base and moving platform are not arbitrarily selected. There are two layout subgroups among which base and moving platform layouts can be matched with each other. The two main subgroups are the ones generated from U^T, U^N, U^{VT}, U^{VN} and U^X, U^Y, U^{VX}, U^{VY}. Under these conditions, the sub-joint layouts are derived. For U^T, U^N, U^{VT} and U^{VN} the sub-joint layouts can be seen in Fig. 4. Sub-joint layouts for U^X, U^Y, U^{VX} and U^{VY} joint layouts are shown in Fig. 5.

At this point, we present the whole list of assumptions for the joint layouts of the 3-UPU PMs to be classified:

- The base and the moving platform triangles are equilateral.

https://doi.org/10.1017/S0263574721001259 Published online by Cambridge University Press

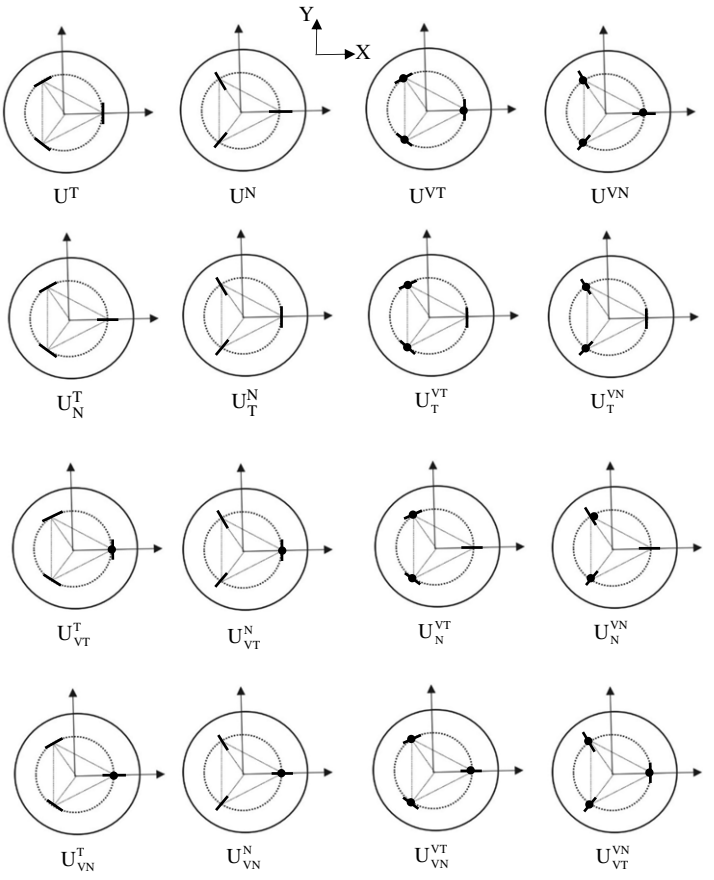


Figure 4. *Sub-joint layouts for U^T, U^N, U^{VT} and U^{VN}.*

In order to define the relative joint locations, an initial configuration of the PM is set. At the initial configuration of the PM:

- The moving platform plane is parallel to the base platform plane.
- The center of the moving platform triangle is on the Z-axis of the GCS which is located at the center of the base platform triangle with Z-axis perpendicular to the base platform plane. Therefore, all three limbs make the same angle with the base platform plane.
- If the joint axis associated with a platform are on the platform plane, the joint axes are either tangent (denoted by T) or normal (denoted by N) to the circumcircle of the platform triangle, or else they are parallel to either X-axis (denoted by X) or Y-axis (denoted by Y) of the GCS.
- If the joint axis associated with a platform is perpendicular (V) to the platform plane, the consecutive joint axes are either tangent (denoted by VT) or normal (denoted by VN) to the circumcircle of the platform triangle, or else they are parallel to either X-axis (denoted by VX) or Y-axis (denoted by VY) of the GCS. As a consequence of this assumption, if any of the consecutive joint axes are not tangent to the circumcircle of the platform triangle, then the associated limb has to be perpendicular to the platform and hence the platforms are necessarily identical.
- A platform's sub-joint layout is obtained by only changing the joint type associated with the first limb and keeping the joint type associated with the second and third limbs.

https://doi.org/10.1017/S0263574721001259 Published online by Cambridge University Press

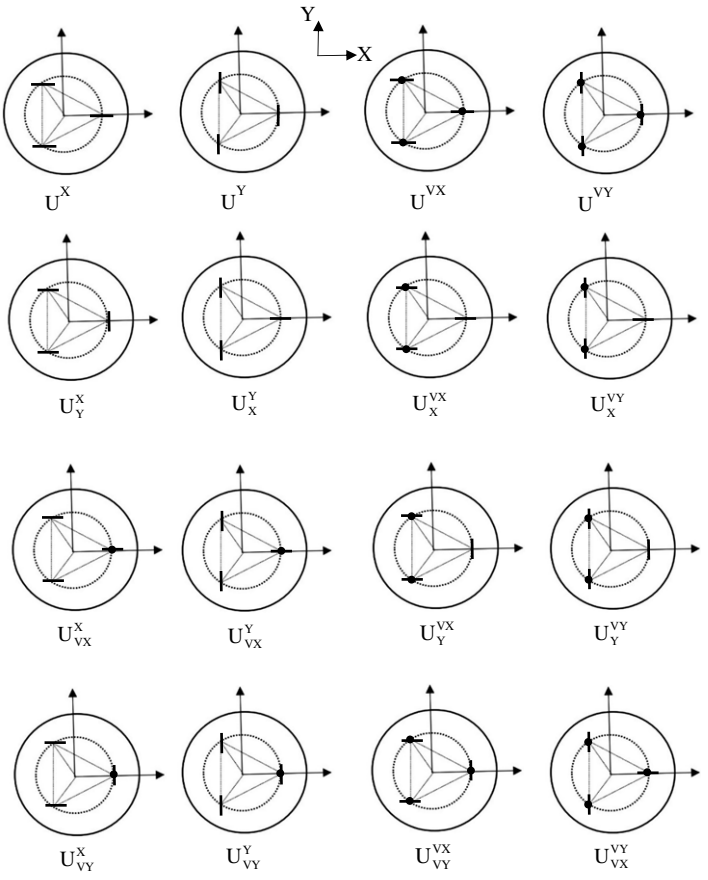


Figure 5. *Sub-joint layouts for U^X, U^Y, U^{VX} and U^{VY}.*

2.3. Novel 3-UPU PMs consisting of sub-joint layouts

Created sub-joint layouts are matched with each other as base and moving platforms under two main groups: TNV group presented in Fig. 4 and XYV group presented in Fig. 5. Since there are 16 different sub-joint layouts in each group, a 16-by-16 table was created and 256 different PMs were derived for each group. In Section 3, the initial configurations of the PMs are taken into consideration while analyzing the mobility of the PM. To proceed with the mobility analysis, limb types are classified according to the locations of the joints on the limb in the initial configuration of the PM. Accordingly, the limbs of the TNV-type PMs are located in the xz-planes of the LCSs in the initial configuration. In XYV-type manipulators, limbs are assumed to be along the z-axes of the LCSs. Therefore, for XYV-type PMs the base and the moving platforms are assumed to be identical, because in the literature there are no XYV-type PMs with non-identical platforms and such a PM would not be a practical one. Under these assumptions, after the base and mobile platform layouts are matched to each other, it is seen that there are 16 different limb types in total (Table II). The limb types are divided into four main groups according to the locations of the R_{i1} and R_{i2} axes of each limb in the LCS in the initial configuration of the PM. These groups are defined such that the R_{i1} or R_{i2} axes are along the x-, y- or z-axis of the LCS.

The limb types with R_{i1} axis parallel to the y-axis of the LCS are designated as R_y-. There are four sub-types according to the joint locations on the moving platform. As shown in Fig. 6(a), the limb type where the R_{i5} axis is parallel to the y-axis of the LCS is designated as R_y–R_y. If the R_{i5} axis is parallel to the x-axis of the LCS, this kind of limb is denoted as R_y–R_x (Fig. 6(b)). When R_{i5} axis is parallel to the z-axis of the LCS and R_{i4} axis is parallel to the y-axis of the LCS in the initial configuration of the

https://doi.org/10.1017/S0263574721001259 Published online by Cambridge University Press

Table II. *Symbolic equivalents of limb types*

k_1	k_2	k_3	k_4	k_5	k_6	k_7	k_8
R_y–R_y	R_y–R_x	R_y–R_yR_z	R_y–R_xR_z	R_x–R_y	R_x–R_x	R_x–R_yR_z	R_x–R_xR_z
k_9	k_{10}	k_{11}	k_{12}	k_{13}	k_{14}	k_{15}	k_{16}
R_zR_y–R_y	R_zR_y–R_x	R_zR_y–R_yR_z	R_zR_y–R_xR_z	R_zR_x–R_y	R_zR_x–R_x	R_zR_x–R_yR_z	R_zR_x–R_xR_z

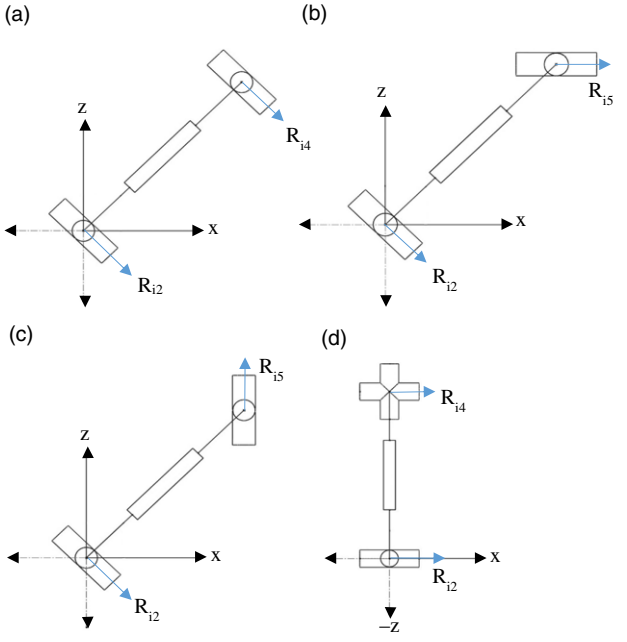


Figure 6. *R_y-type limbs (a) R_y–R_y, (b) R_y–R_x, (c) R_y–R_yR_z, (d) R_y–R_xR_z.*

PM, it is shown as R_y–R_yR_z (Fig. 6(c)), whereas if R_{i4} axis is parallel to the x-axis of LCS in the initial configuration, it is shown as R_y–R_xR_z (Fig. 6(d)).

The limb types with R_{i1} axis parallel to the x-axis of the LCS are designated as R_x-. Since the R_{i4} and R_{i5} locations are the same as R_y-type limbs, the representation of second part after the P joint is similar (Fig. 7).

The limb types with R_{i1} axis parallel to the z-axis and R_{i2} axis parallel to the y-axis of the LCS are designated as R_zR_y-. As shown in Fig. 8(a), the limb type with R_{i5} axis parallel to the y-axis of the LCS is designated as R_zR_y–R_y. If R_{i5} axis is parallel to the x-axis of the LCS, this kind of limb is denoted as R_zR_y-R_x (Fig. 8(b)). When R_{i5} axis is parallel to the z-axis of the LCS and R_{i4} axis is parallel to the y-axis of the LCS in the initial configuration of the PM, it is shown as R_zR_y–R_yR_z (Fig. 8(c)) whereas if R_{i4} axis is parallel to the x-axis of LCS, it is shown as R_zR_y–R_xR_z (Fig. 8(d)). The limb types with R_{i1} axis parallel to the z-axis and R_{i2} axis parallel to the x-axis of the LCS are designated as R_zR_x-. Since the R_{i4} and R_{i5} locations are the same as R_zR_y-type limbs, the representation of second part after the P joint is similar (Fig. 9).

There are totally 16 limb types described in the previous subsections. For brevity, these limb types are designated with k_i for $i = 1, \ldots, 16$ as given in Table II.

2.4. Joint layout matching

When a base and a moving platform of given joint layout are matched with each other, the limp types will be one of the 16 types given in Table II. As it is assumed that limbs 2 and 3 need to be identical

https://doi.org/10.1017/S0263574721001259 Published online by Cambridge University Press

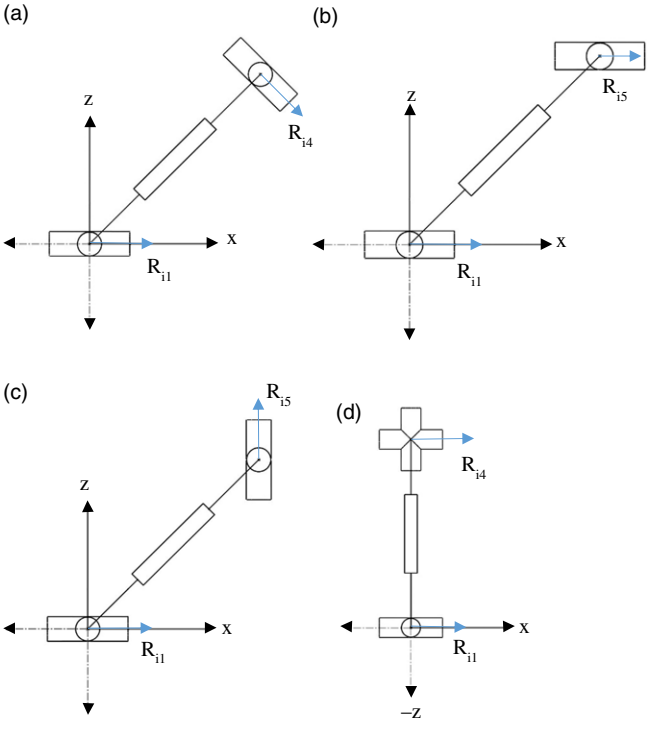


Figure 7. *R_x-type limbs (a) R_x–R_y, (b) R_x–R_x, (c) R_x–R_yR_z, (d) R_x–R_xR_z.*

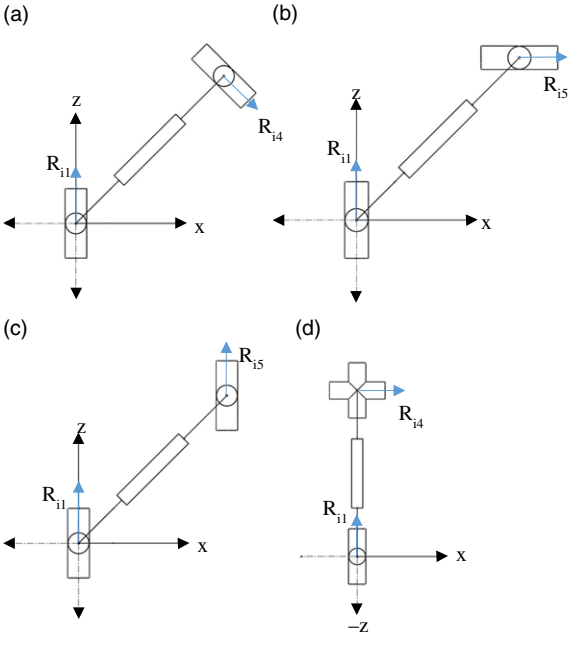


Figure 8. *R_zR_y-type limbs (a) R_zR_y–R_y, (b) R_zR_y–R_x, (c) R_zR_y–R_yR_z, (d) R_zR_y–R_xR_z.*

https://doi.org/10.1017/S0263574721001259 Published online by Cambridge University Press

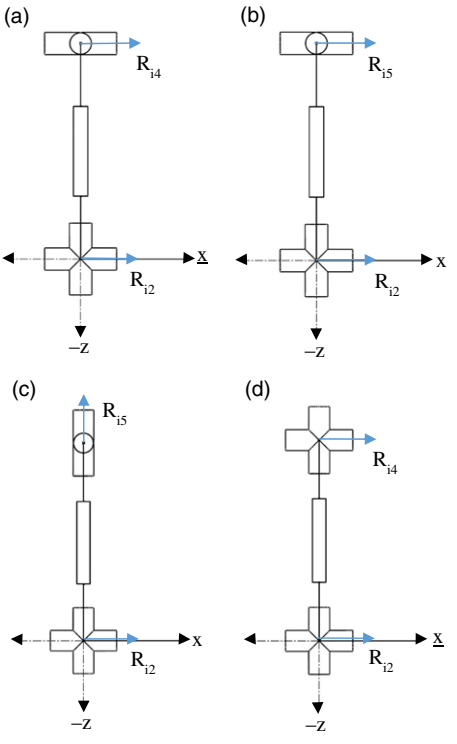


Figure 9. *R_zR_x-type limbs (a) R_zR_x–R_y, (b) R_zR_x–R_x, (c) R_zR_x–R_yR_z, (d) R_zR_x–R_xR_z.*

while limb 1 can be different, the limbs of the TNV-type and XYV-type platforms can be classified as given in Tables III, IV, V and VI. As an example, when a U_T^{VT} base and a U_N^T moving platform are matched, limb 1 type is k_2 (from Table II) and limbs 2 and 3 type is k_9 (from Table III). By this way, it can be seen that there are 256 TNV-type PMs (each element of Tables II or III) and 256 XYV-type PMs (each element of Tables IV or V). The mobility analysis of all PMs is performed in Section 4 based on the theory presented in Section 3.

3. Joint screws of the limbs

In this section, the screw system of the limb types described in Section 2 are presented. The locations of the joint axes and the limb axes in between the universal joint centers at the terminals of the limb in the initial configuration of the PM are considered. In the initial configuration of a TNV-type PM, the limb axes are always on the xz-plane of their respective LCSs. Meanwhile, in the initial configuration of an XYV-type PM, the limb axes are along the z-axis of their respective LCSs. The angle between the limb axis and the x-axis on the xz-plane in the initial configuration of the PM is denoted by θ and limb length is denoted by l. For the TNV-type PMs, typical values of θ are used for mobility analysis: 0°, 30°, 45°, 60°, 90°. These values correspond to the cases which result in PMs with extra mobility in the literature [28].

As seen in Fig. 10, the R_{i1} joint axes of the R_y-type limbs are along the y-axis of the LCS on the base (In Figs. 10, 11, 12 and 13 $\otimes$ represents a screw axis along the y-axis, i.e. perpendicular to the xz-plane). For this reason, as seen in Table VII, the primary part of the first screws of the R_y-type limbs are unit vectors along the y-axis. In Table VII, c and s are abbreviations of cosine and sine, respectively. For the second screws, R_{i2} joint axes of the R_y–R_y, R_y–R_x and R_y–R_yR_z limbs are located on the xz-plane, whereas the R_y–R_xR_z limb has to be along the x-axis of the LCS in the initial configuration of the PM.

https://doi.org/10.1017/S0263574721001259 Published online by Cambridge University Press

Table III. *Limb types of first limbs of TNV-type PMs*

		MOVING PLATFORM															
Limb-1		U^T	U^N	U^{VT}	U^{VN}	U^T_N	U^N_T	U^{VT}_T	U^{VN}_T	U^{VT}_N	U^{VN}_N	U^T_{VT}	U^T_{VN}	U^N_{VT}	U^N_{VN}	U^{VT}_{VN}	U^{VN}_{VT}
	U^T	k_1	k_2	k_3	k_4	k_2	k_1	k_1	k_1	k_2	k_2	k_3	k_4	k_3	k_4	k_4	k_3
	U^N	k_5	k_6	k_7	k_8	k_6	k_5	k_5	k_5	k_6	k_6	k_7	k_8	k_7	k_8	k_8	k_7
	U^{VT}	k_9	k_{10}	k_{11}	k_{12}	k_{10}	k_9	k_9	k_9	k_{10}	k_{10}	k_{11}	k_{12}	k_{11}	k_{12}	k_{12}	k_{11}
	U^{VN}	k_{13}	k_{14}	k_{15}	k_{16}	k_{14}	k_{13}	k_{13}	k_{13}	k_{14}	k_{14}	k_{15}	k_{16}	k_{15}	k_{16}	k_{16}	k_{15}
	U^T_N	k_5	k_6	k_7	k_8	k_6	k_5	k_5	k_5	k_6	k_6	k_7	k_8	k_7	k_8	k_8	k_7
	U^N_T	k_1	k_2	k_3	k_4	k_2	k_1	k_1	k_1	k_2	k_2	k_3	k_4	k_3	k_4	k_4	k_3
	U^{VT}_T	k_1	k_2	k_3	k_4	k_2	k_1	k_1	k_1	k_2	k_2	k_3	k_4	k_3	k_4	k_4	k_3
BASE	U^{VN}_T	k_1	k_2	k_3	k_4	k_2	k_1	k_1	k_1	k_2	k_2	k_3	k_4	k_3	k_4	k_4	k_3
	U^{VT}_N	k_5	k_6	k_7	k_8	k_6	k_5	k_5	k_5	k_6	k_6	k_7	k_8	k_7	k_8	k_8	k_7
	U^{VN}_N	k_5	k_6	k_7	k_8	k_6	k_5	k_5	k_5	k_6	k_6	k_7	k_8	k_7	k_8	k_8	k_7
	U^T_{VT}	k_9	k_{10}	k_{11}	k_{12}	k_{10}	k_9	k_9	k_9	k_{10}	k_{10}	k_{11}	k_{12}	k_{11}	k_{12}	k_{12}	k_{11}
	U^T_{VN}	k_{13}	k_{14}	k_{15}	k_{16}	k_{14}	k_{13}	k_{13}	k_{13}	k_{14}	k_{14}	k_{15}	k_{16}	k_{15}	k_{16}	k_{16}	k_{15}
	U^N_{VT}	k_9	k_{10}	k_{11}	k_{12}	k_{10}	k_9	k_9	k_9	k_{10}	k_{10}	k_{11}	k_{12}	k_{11}	k_{12}	k_{12}	k_{11}
	U^N_{VN}	k_{13}	k_{14}	k_{15}	k_{16}	k_{14}	k_{13}	k_{13}	k_{13}	k_{14}	k_{14}	k_{15}	k_{16}	k_{15}	k_{16}	k_{16}	k_{15}
	U^{VT}_{VN}	k_{13}	k_{14}	k_{15}	k_{16}	k_{14}	k_{13}	k_{13}	k_{13}	k_{14}	k_{14}	k_{15}	k_{16}	k_{15}	k_{16}	k_{16}	k_{15}
	U^{VN}_{VT}	k_9	k_{10}	k_{11}	k_{12}	k_{10}	k_9	k_9	k_9	k_{10}	k_{10}	k_{11}	k_{12}	k_{11}	k_{12}	k_{12}	k_{11}

Table IV. *Limb types of second and third limbs of TNV-type PMs*

		MOVING PLATFORM															
Limbs 2 and 3		U^T	U^N	U^{VT}	U^{VN}	U^T_N	U^N_T	U^{VT}_T	U^{VN}_T	U^{VT}_N	U^{VN}_N	U^T_{VT}	U^T_{VN}	U^N_{VT}	U^N_{VN}	U^{VT}_{VN}	U^{VN}_{VT}
	U^T	k_1	k_2	k_3	k_4	k_1	k_2	k_3	k_4	k_3	k_4	k_1	k_1	k_2	k_2	k_3	k_4
	U^N	k_5	k_6	k_7	k_8	k_5	k_6	k_7	k_8	k_7	k_8	k_5	k_5	k_6	k_6	k_7	k_8
	U^{VT}	k_9	k_{10}	k_{11}	k_{12}	k_9	k_{10}	k_{11}	k_{12}	k_{11}	k_{12}	k_9	k_9	k_{10}	k_{10}	k_{11}	k_{12}
	U^{VN}	k_{13}	k_{14}	k_{15}	k_{16}	k_{13}	k_{14}	k_{15}	k_{16}	k_{15}	k_{16}	k_{13}	k_{13}	k_{14}	k_{14}	k_{15}	k_{16}
	U^T_N	k_1	k_2	k_3	k_4	k_1	k_2	k_3	k_4	k_3	k_4	k_1	k_1	k_2	k_2	k_3	k_4
	U^N_T	k_5	k_6	k_7	k_8	k_5	k_6	k_7	k_8	k_7	k_8	k_5	k_5	k_6	k_6	k_7	k_8
BASE	U^{VT}_T	k_9	k_{10}	k_{11}	k_{12}	k_9	k_{10}	k_{11}	k_{12}	k_{11}	k_{12}	k_9	k_9	k_{10}	k_{10}	k_{11}	k_{12}
	U^{VN}_T	k_{13}	k_{14}	k_{15}	k_{16}	k_{13}	k_{14}	k_{15}	k_{16}	k_{15}	k_{16}	k_{13}	k_{13}	k_{14}	k_{14}	k_{15}	k_{16}
	U^{VT}_N	k_9	k_{10}	k_{11}	k_{12}	k_9	k_{10}	k_{11}	k_{12}	k_{11}	k_{12}	k_9	k_9	k_{10}	k_{10}	k_{11}	k_{12}
	U^{VN}_N	k_{13}	k_{14}	k_{15}	k_{16}	k_{13}	k_{14}	k_{15}	k_{16}	k_{15}	k_{16}	k_{13}	k_{13}	k_{14}	k_{14}	k_{15}	k_{16}
	U^T_{VT}	k_1	k_2	k_3	k_4	k_1	k_2	k_3	k_4	k_3	k_4	k_1	k_1	k_2	k_2	k_3	k_4
	U^T_{VN}	k_1	k_2	k_3	k_4	k_1	k_2	k_3	k_4	k_3	k_4	k_1	k_1	k_2	k_2	k_3	k_4
	U^N_{VT}	k_5	k_6	k_7	k_8	k_5	k_6	k_7	k_8	k_7	k_8	k_5	k_5	k_6	k_6	k_7	k_8
	U^N_{VN}	k_5	k_6	k_7	k_8	k_5	k_6	k_7	k_8	k_7	k_8	k_5	k_5	k_6	k_6	k_7	k_8
	U^{VT}_{VN}	k_9	k_{10}	k_{11}	k_{12}	k_9	k_{10}	k_{11}	k_{12}	k_{11}	k_{12}	k_9	k_9	k_{10}	k_{10}	k_{11}	k_{12}
	U^{VN}_{VT}	k_{13}	k_{14}	k_{15}	k_{16}	k_{13}	k_{14}	k_{15}	k_{16}	k_{15}	k_{16}	k_{13}	k_{13}	k_{14}	k_{14}	k_{15}	k_{16}

Hence, the primary part of the second screw of R_y–R_xR_z limb is the unit vector along the x-axis of the LCS. Likewise, for the third screws of R_y–R_xR_z limb, R_{i3} joint direction has to be along the z-axis of the LCS on the base, whereas R_{i3} joint directions of the rest of the limbs are on the xz-plane. The prismatic joint corresponds to infinite-pitch screws, so the secondary part of the third screw of the R_y–R_xR_z limb is unit vector along the z-axis, whereas it is on the xz-plane for the rest of the limbs.

For R_y–R_y limb, the primary part of the fourth screw is identical to the second screw of R_y–R_y limb. The fourth screws for R_y–R_x and R_y–R_yR_z limbs are identical to each other and the primary parts are

https://doi.org/10.1017/S0263574721001259 Published online by Cambridge University Press

Table V. *Limb types of first limbs of XYV-type PMs*

		MOVING PLATFORM															
Limb-1		U^{X}	U^{Y}	U^{VX}	U^{VY}	U^{X}_{Y}	U^{Y}_{X}	U^{VX}_{X}	U^{VY}_{X}	U^{VX}_{Y}	U^{VY}_{Y}	U^{X}_{VX}	U^{X}_{VY}	U^{Y}_{VX}	U^{Y}_{VY}	U^{VX}_{VY}	U^{VY}_{VX}
	U^{X}	k_6	k_5	k_8	k_7	k_5	k_6	k_6	k_6	k_8	k_7	k_8	k_7	k_5	k_5	k_7	k_8
	U^{Y}	k_2	k_1	k_4	k_3	k_1	k_2	k_2	k_2	k_4	k_3	k_4	k_3	k_1	k_1	k_3	k_4
	U^{VX}	k_{14}	k_{13}	k_{16}	k_{15}	k_{13}	k_{14}	k_{14}	k_{14}	k_{16}	k_{15}	k_{16}	k_{15}	k_{13}	k_{13}	k_{15}	k_{16}
	U^{VY}	k_{10}	k_9	k_{12}	k_{11}	k_9	k_{10}	k_{10}	k_{10}	k_{12}	k_{11}	k_{12}	k_{11}	k_9	k_9	k_{11}	k_{12}
	U^{X}_{Y}	k_2	k_1	k_4	k_3	k_1	k_2	k_2	k_2	k_4	k_3	k_4	k_3	k_1	k_1	k_3	k_4
	U^{Y}_{X}	k_6	k_5	k_8	k_7	k_5	k_6	k_6	k_6	k_8	k_7	k_8	k_7	k_5	k_5	k_7	k_8
	U^{VX}_{X}	k_6	k_5	k_8	k_7	k_5	k_6	k_6	k_6	k_8	k_7	k_8	k_7	k_5	k_5	k_7	k_8
	U^{VY}_{X}	k_6	k_5	k_8	k_7	k_5	k_6	k_6	k_6	k_8	k_7	k_8	k_7	k_5	k_5	k_7	k_8
BASE	U^{VX}_{Y}	k_{14}	k_{13}	k_{16}	k_{15}	k_{13}	k_{14}	k_{14}	k_{14}	k_{16}	k_{15}	k_{16}	k_{15}	k_{13}	k_{13}	k_{15}	k_{16}
	U^{VY}_{Y}	k_{10}	k_9	k_{12}	k_{11}	k_9	k_{10}	k_{10}	k_{10}	k_{12}	k_{11}	k_{12}	k_{11}	k_9	k_9	k_{11}	k_{12}
	U^{X}_{VX}	k_{14}	k_{13}	k_{16}	k_{15}	k_{13}	k_{14}	k_{14}	k_{14}	k_{16}	k_{15}	k_{16}	k_{15}	k_{13}	k_{13}	k_{15}	k_{16}
	U^{X}_{VY}	k_{10}	k_9	k_{12}	k_{11}	k_9	k_{10}	k_{10}	k_{10}	k_{12}	k_{11}	k_{12}	k_{11}	k_9	k_9	k_{11}	k_{12}
	U^{Y}_{VX}	k_2	k_1	k_4	k_3	k_1	k_2	k_2	k_2	k_4	k_3	k_4	k_3	k_1	k_1	k_3	k_4
	U^{Y}_{VY}	k_2	k_1	k_4	k_3	k_1	k_2	k_2	k_2	k_4	k_3	k_4	k_3	k_1	k_1	k_3	k_4
	U^{VX}_{VY}	k_{10}	k_9	k_{12}	k_{11}	k_9	k_{10}	k_{10}	k_{10}	k_{12}	k_{11}	k_{12}	k_{11}	k_9	k_9	k_{11}	k_{12}
	U^{VY}_{VX}	k_{14}	k_{13}	k_{16}	k_{15}	k_{13}	k_{14}	k_{14}	k_{14}	k_{16}	k_{15}	k_{16}	k_{15}	k_{13}	k_{13}	k_{15}	k_{16}

Table VI. *Limb types of second and third limbs of XYV-type PMs*

		MOVING PLATFORM															
Limbs 2 and 3		U^{X}	U^{Y}	U^{VX}	U^{VY}	U^{X}_{Y}	U^{Y}_{X}	U^{VX}_{X}	U^{VY}_{X}	U^{VX}_{Y}	U^{VY}_{Y}	U^{X}_{VX}	U^{X}_{VY}	U^{Y}_{VX}	U^{Y}_{VY}	U^{VX}_{VY}	U^{VY}_{VX}
	U^{X}	k_6	k_5	k_8	k_7	k_6	k_5	k_8	k_7	k_6	k_6	k_5	k_5	k_8	k_7	k_8	k_7
	U^{Y}	k_2	k_1	k_4	k_3	k_2	k_1	k_4	k_3	k_2	k_2	k_1	k_1	k_4	k_3	k_4	k_3
	U^{VX}	k_{14}	k_{13}	k_{16}	k_{15}	k_{14}	k_{13}	k_{16}	k_{15}	k_{14}	k_{14}	k_{13}	k_{13}	k_{16}	k_{15}	k_{16}	k_{15}
	U^{VY}	k_{10}	k_9	k_{12}	k_{11}	k_{10}	k_9	k_{12}	k_{11}	k_{10}	k_{10}	k_9	k_9	k_{12}	k_{11}	k_{12}	k_{11}
	U^{X}_{Y}	k_6	k_5	k_8	k_7	k_6	k_5	k_8	k_7	k_6	k_6	k_5	k_5	k_8	k_7	k_8	k_7
	U^{Y}_{X}	k_2	k_1	k_4	k_3	k_2	k_1	k_4	k_3	k_2	k_2	k_1	k_1	k_4	k_3	k_4	k_3
	U^{VX}_{X}	k_{14}	k_{13}	k_{16}	k_{15}	k_{14}	k_{13}	k_{16}	k_{15}	k_{14}	k_{14}	k_{13}	k_{13}	k_{16}	k_{15}	k_{16}	k_{15}
BASE	U^{VY}_{X}	k_{10}	k_9	k_{12}	k_{11}	k_{10}	k_9	k_{12}	k_{11}	k_{10}	k_{10}	k_9	k_9	k_{12}	k_{11}	k_{12}	k_{11}
	U^{VX}_{Y}	k_6	k_5	k_8	k_7	k_6	k_5	k_8	k_7	k_6	k_6	k_5	k_5	k_8	k_7	k_8	k_7
	U^{VY}_{Y}	k_6	k_5	k_8	k_7	k_6	k_5	k_8	k_7	k_6	k_6	k_5	k_5	k_8	k_7	k_8	k_7
	U^{X}_{VX}	k_2	k_1	k_4	k_3	k_2	k_1	k_4	k_3	k_2	k_2	k_1	k_1	k_4	k_3	k_4	k_3
	U^{X}_{VY}	k_2	k_1	k_4	k_3	k_2	k_1	k_4	k_3	k_2	k_2	k_1	k_1	k_4	k_3	k_4	k_3
	U^{Y}_{VX}	k_{14}	k_{13}	k_{16}	k_{15}	k_{14}	k_{13}	k_{16}	k_{15}	k_{14}	k_{14}	k_{13}	k_{13}	k_{16}	k_{15}	k_{16}	k_{15}
	U^{Y}_{VY}	k_{10}	k_9	k_{12}	k_{11}	k_{10}	k_9	k_{12}	k_{11}	k_{10}	k_{10}	k_9	k_9	k_{12}	k_{11}	k_{12}	k_{11}
	U^{VX}_{VY}	k_{14}	k_{13}	k_{16}	k_{15}	k_{14}	k_{13}	k_{16}	k_{15}	k_{14}	k_{14}	k_{13}	k_{13}	k_{16}	k_{15}	k_{16}	k_{15}
	U^{VY}_{VX}	k_{10}	k_9	k_{12}	k_{11}	k_{10}	k_9	k_{12}	k_{11}	k_{10}	k_{10}	k_9	k_9	k_{12}	k_{11}	k_{12}	k_{11}

the same as the first screws. For the R_y–R_xR_z limb the primary part of the fourth screw is unit vector along x-axis in the initial configuration of the PM. R_{i5} joint axis of R_y–R_y limb is parallel to the y-axis of the LCS and the primary part of the fifth screw of R_y–R_y limb is unit vector along the y-axis in the initial configuration of the PM. R_{i5} joint axis of R_y–R_x limb is parallel to the x-axis of the LCS and the primary part of the fifth screw of R_y–R_x limb is unit vector along the x-axis in the initial configuration of the PM. For the R_y–R_yR_z and R_y–R_xR_z limbs, the primary part of the fifth screws of R_y–R_yR_z and

https://doi.org/10.1017/S0263574721001259 Published online by Cambridge University Press

Table VII. *Screws of R_y-type limbs (R_y–R_y, R_y–R_x, R_y–R_yR_z, R_y–R_xR_z)*

	R_y–R_y	R_y–R_x	R_y–R_yR_z	R_y–R_xR_z
$\$_1$	(0, 1, 0; 0, 0, 0)	(0, 1, 0; 0, 0, 0)	(0, 1, 0; 0, 0, 0)	(0, 1, 0; 0, 0, 0)
$\$_2$	(sθ, 0, -cθ; 0, 0, 0)	(sθ, 0, -cθ; 0, 0, 0)	(sθ, 0, -cθ; 0, 0, 0)	(1, 0, 0; 0, 0, 0)
$\$_3$	(0, 0, 0; cθ, 0, sθ)	(0, 0, 0; cθ, 0, sθ)	(0, 0, 0; cθ, 0, sθ)	(0, 0, 0; 0, 0, 1)
$\$_4$	(sθ, 0, -cθ; 0, l, 0)	(0, 1, 0; -lsθ, 0, lcθ)	(0, 1, 0; -lsθ, 0, lcθ)	(1, 0, 0; 0, l, 0)
$\$_5$	(0, 1, 0; -lsθ, 0, lcθ)	(1, 0, 0; 0, lsθ, 0)	(0, 0, 1; 0, -lcθ, 0)	(0, 0, 1; 0, 0, 0)

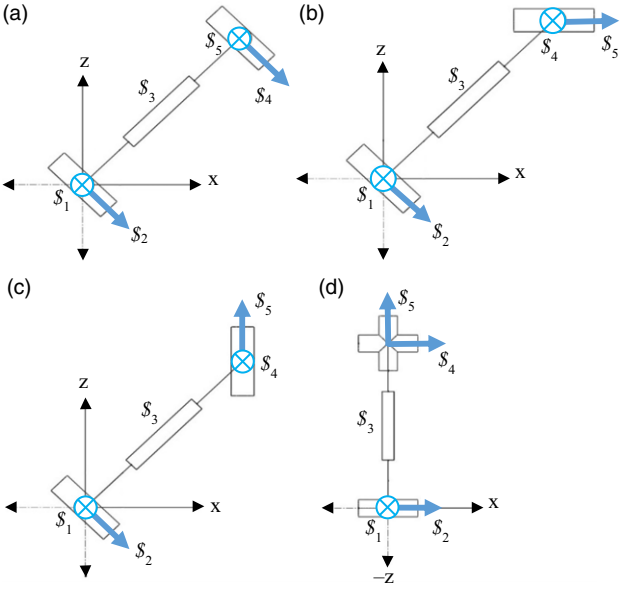


Figure 10. *Screws of R_y-type limbs (a) R_y–R_y, (b) R_y–R_x, (c) R_y–R_yR_z, (d) R_y–R_xR_z.*

R_y–R_xR_z limbs are unit vectors along the z-axis. The screws of R_y-type limbs are given in Table VII in detail.

The R_{i1} joint axes of the R_x-type limbs are along the x-axis of the LCS on the base (Fig. 11). For this reason, as seen in Table VIII, the primary parts of the first screws of the R_x-type limbs are unit vectors along the x-axis. For the second screws, R_{i2} joint axes of the R_x–R_y, R_x–R_x, R_x–R_yR_z and R_x–R_xR_z limbs are along the y-axis of the LCS on the base in the initial configuration of the PM, so the primary parts of the screws are unit vectors along the y-axis. The third screws of the R_y-type limbs are the same as the third screws of the R_x-type limbs. For the R_x–R_y limb, the primary part of the fourth screw is identical to the second screw of the R_y–R_y limb. The fourth screws for R_x–R_x and R_x–R_yR_z limbs are identical to each other and the primary parts are the same as the second screws. For the R_x–R_xR_z limb, the primary part of the fourth screw is unit vector along the x-axis in the initial configuration of the PM. The primary part of the fifth screw of R_x–R_y is unit vector along the y-axis in the initial configuration of the PM. The primary part of the fifth screw of the R_y–R_x limb is unit vector along the x-axis in the initial configuration of the PM. For the R_x–R_yR_z and R_x–R_xR_z, R_{i5} limbs the primary part of the fifth screw is unit vector along the z-axis. The screws of R_x-type limbs are given in Table VIII in detail.

The R_{i1} joint axes of the R_zR_y-type limbs are along the z-axis of the LCS on the base (Fig. 12). For this reason, as seen in Table IX, the first screws of the R_zR_y-type limbs are unit vectors along the z-axis. For the second screws, R_{i2} joint axes of the R_zR_y–R_y, R_zR_y–R_x, R_zR_y–R_yR_z and R_zR_y–R_xR_z limbs are along the y-axis of the LCS on the base in the initial configuration of the PM and the primary part of screws are unit vectors along the y-axis. The third screws of the R_zR_y-type limbs are the same as the third

https://doi.org/10.1017/S0263574721001259 Published online by Cambridge University Press

Table VIII. *Screws of R_x-type limbs (R_x–R_y, R_x–R_x, R_x–R_yR_z, R_x–R_xR_z)*

	$\mathbf{R_x–R_y}$	$\mathbf{R_x–R_x}$	$\mathbf{R_x–R_yR_z}$	$\mathbf{R_x–R_xR_z}$
$\$_1$	(1, 0, 0; 0, 0, 0)	(1, 0, 0; 0, 0, 0)	(1, 0, 0; 0, 0, 0)	(1, 0, 0; 0, 0, 0)
$\$_2$	(0, 1, 0; 0, 0, 0)	(0, 1, 0; 0, 0, 0)	(0, 1, 0; 0, 0, 0)	(0, 1, 0; 0, 0, 0)
$\$_3$	(0, 0, 0; cθ, 0, sθ)	(0, 0, 0; cθ, 0, sθ)	(0, 0, 0; cθ, 0, sθ)	(0, 0, 0; 0, 0, 1)
$\$_4$	(sθ, 0, -cθ; 0, l, 0)	(0, 1, 0; -lsθ, 0, lcθ)	(0, 1, 0; -lsθ, 0, lcθ)	(1, 0, 0; 0, l, 0)
$\$_5$	(0, 1, 0; -lsθ, 0, lcθ)	(1, 0, 0; 0, lsθ, 0)	(0, 0, 1; 0, -lcθ, 0)	(0, 0, 1; 0, 0, 0)

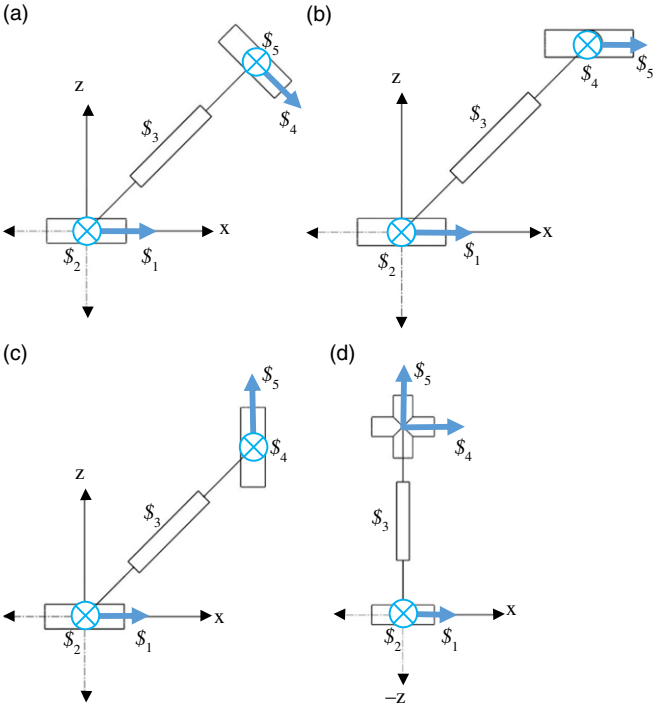


Figure 11. *Screws of R_x-type limbs (a) R_x–R_y, (b) R_x–R_x, (c) R_x–R_yR_z, (d) R_x–R_xR_z.*

screws of the R_x-type limbs. For R_zR_y–R_y limb, the primary part of the fourth screw is identical to the second screw of R_y–R_y limb. The fourth screws for R_zR_y–R_x and R_zR_y–R_yR_z limbs are identical to each other and the primary parts are the same as the second screws. For the R_zR_y–R_xR_z limb, the primary part of the fourth screw is unit vector along the x-axis in the initial configuration of the PM. R_{i5} joint axis of the R_zR_y–R_y limb is parallel to the y-axis of LCS and the primary part of the fifth screw of the R_zR_y–R_y limb is unit vector along the y-axis in the initial configuration of the PM. R_{i5} joint axis of the R_zR_y–R_x limb is parallel to the x-axis of LCS and the primary part of the fifth screw of the R_zR_y–R_x limb is unit vector along the x-axis in the initial configuration of the PM. For the R_zR_y–R_yR_z and R_zR_y–R_xR_z limbs, the primary part of the fifth screw is unit vector along the z-axis. The screws of R_zR_y-type limbs are given in Table IX in detail.

The R_{i1} joint axes of the R_zR_x-type limbs are along the z-axis of the LCS on the base (Fig. 13). For this reason, as seen in Table X, the first screws of the R_zR_x-type limbs are unit vectors along the z-axis. For R_{i2} joint axes of the R_zR_x–R_y, R_zR_x–R_x, R_zR_x–R_yR_z and R_zR_x–R_xR_z limbs the primary part of screws are unit vectors along the x-axis. For the third screws of R_zR_x-type limbs, R_{i3} joint axes has to be positioned along the z-axis of the LCS on the base in the initial configuration of the PM. For R_zR_x–R_y

https://doi.org/10.1017/S0263574721001259 Published online by Cambridge University Press

Table IX. *Screws of R_zR_y-type limbs R_zR_y–R_y, R_zR_y–R_x, R_zR_y–R_yR_z, R_zR_y–R_xR_z*

	$\mathbf{R_zR_y}$–$\mathbf{R_y}$	$\mathbf{R_zR_y}$–$\mathbf{R_x}$	$\mathbf{R_zR_y}$–$\mathbf{R_yR_z}$	$\mathbf{R_zR_y}$–$\mathbf{R_xR_z}$
$\$_1$	(0, 0, 1; 0, 0, 0)	(0, 0, 1; 0, 0, 0)	(0, 0, 1; 0, 0, 0)	(0, 0, 1; 0, 0, 0)
$\$_2$	(0, 1, 0; 0, 0, 0)	(0, 1, 0; 0, 0, 0)	(0, 1, 0; 0, 0, 0)	(0, 1, 0; 0, 0, 0)
$\$_3$	(0, 0, 0; cθ, 0, sθ)	(0, 0, 0; cθ, 0, sθ)	(0, 0, 0; cθ, 0, sθ)	(0, 0, 0; 0, 0, 1)
$\$_4$	(sθ, 0, -cθ; 0, l, 0)	(0, 1, 0; -lsθ, 0, lcθ)	(0, 1, 0; -lsθ, 0, lcθ)	(1, 0, 0; 0, l, 0)
$\$_5$	(0, 1, 0; -lsθ, 0, lcθ)	(1, 0, 0; 0, lsθ, 0)	(0, 0, 1; 0, -lcθ, 0)	(0, 0, 1; 0, 0, 0)

Table X. *Screws of R_zR_x-type limbs R_zR_x–R_y, R_zR_x–R_x, R_zR_x–R_yR_z, R_zR_x–R_xR_z*

	$\mathbf{R_zR_x}$–$\mathbf{R_y}$	$\mathbf{R_zR_x}$–$\mathbf{R_x}$	$\mathbf{R_zR_x}$–$\mathbf{R_yR_z}$	$\mathbf{R_zR_x}$–$\mathbf{R_xR_z}$
$\$_1$	(0, 0, 1;0, 0, 0)	(0, 0, 1; 0, 0, 0)	(0, 0, 1; 0, 0, 0)	(0, 0, 1; 0, 0, 0)
$\$_2$	(1, 0, 0; 0, 0, 0)	(1, 0, 0; 0, 0, 0)	(1, 0, 0; 0, 0, 0)	(1, 0, 0; 0, 0, 0)
$\$_3$	(0, 0, 0; 0, 0, 1)	(0, 0, 0; 0, 0, 1)	(0, 0, 0; 0, 0, 1)	(0, 0, 0; 0, 0, 1)
$\$_4$	(1, 0, 0; 0, l, 0)	(0, 1, 0; -l, 0, 0)	(0, 1, 0; -l, 0, 0)	(1, 0, 0; 0, l, 0)
$\$_5$	(0, 1, 0; -l, 0, 0)	(1, 0, 0; 0, l, 0)	(0, 0, 1; 0, 0, 0)	(0, 0, 1; 0, 0, 0)

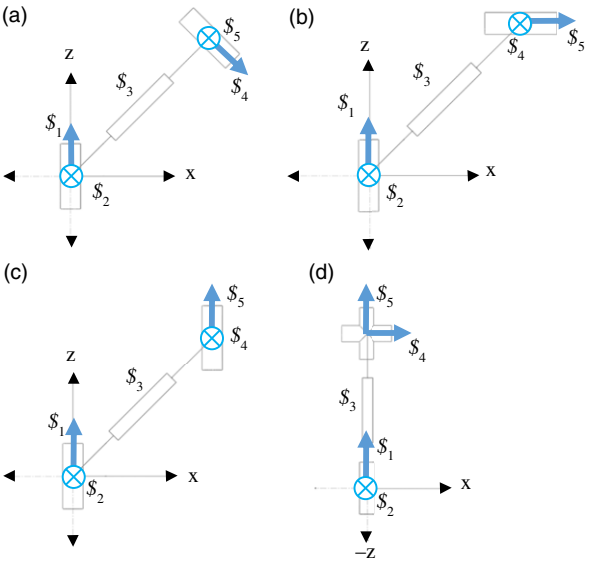


Figure 12. *Screws of R_zR_y-type limbs (a) R_zR_y–R_y, (b) R_zR_y–R_x, (c) R_zR_y–R_yR_z, (d) R_zR_y–R_xR_z.*

and R_zR_x–R_xR_z limbs, the primary part of the fourth screw is identical to the second screw of R_zR_x-type limbs. The fourth screws for R_zR_x–R_x and R_zR_x–R_yR_z limbs are identical to each other and the primary parts are unit vectors along the y-axis. The primary part of the fifth screw of R_zR_x–R_y is unit vector along the y-axis in the initial configuration of the PM. The fifth screw of R_zR_x–R_x is unit vector along the x-axis in the initial configuration of the PM. For the R_zR_x–R_yR_z and R_zR_x–R_xR_z limbs, the primary part of the fifth screw of R_zR_x–R_yR_z and R_zR_x–R_xR_z are unit vector along the z-axis. The screws of R_zR_x-type limbs are given in detail in Table X.

In Section 4, instantaneous mobility analysis of the PMs is performed using the screws of limb types. We also make use of reciprocal screws. For a screw a screw $\$_i = (l_i, m_i, n_i; p_i, q_i, r_i)^{\mathrm{T}}$ and a reciprocal screw of $\$ given by $\$^r = (l^r, m^r, n^r; p^r, q^r, r^r)^{\mathrm{T}}$, the reciprocity condition states that $l_i\, p^r + m_i\, q^r + n_i\, r^r$

https://doi.org/10.1017/S0263574721001259 Published online by Cambridge University Press

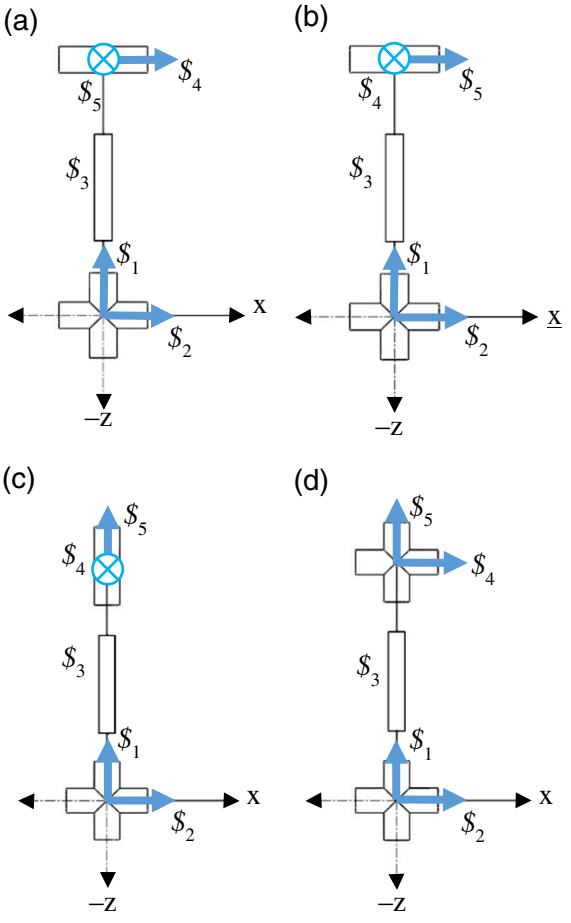


Figure 13. *Screws of R_zR_x-type limbs (a) R_zR_x–R_y, (b) R_zR_x–R_x, (c) R_zR_x–R_yR_z, (d) R_zR_x–R_xR_z.*

$+ p_i\, l^r + q_i\, m^r + r_i\, n^r = 0$. For the 3-UPU PMs, the reciprocal screw of a screw set consisting of five screws is found as

$$\begin{bmatrix} p_1 & q_1 & r_1 & l_1 & m_1 & n_1 \\ p_2 & q_2 & r_2 & l_2 & m_2 & n_2 \\ p_3 & q_3 & r_3 & l_3 & m_3 & n_3 \\ p_4 & q_4 & r_4 & l_4 & m_4 & n_4 \\ p_5 & q_5 & r_5 & l_5 & m_5 & n_5 \end{bmatrix} \begin{bmatrix} l^r \\ m^r \\ n^r \\ p^r \\ q^r \\ r^r \end{bmatrix} = \begin{bmatrix} 0 \\ 0 \\ 0 \\ 0 \\ 0 \\ 0 \end{bmatrix} \tag{35}$$

In order to find a reciprocal screw for a limb, Dai and Jones [76] have developed a practical equation to solve reciprocal of a five screw system:

$$\$^r = (|\mathbf{A}_4|, -|\mathbf{A}_5|, |\mathbf{A}_6|; -|\mathbf{A}_1|, |\mathbf{A}_4|, -|\mathbf{A}_3|)|\mathbf{A}_4|^{\mathrm{T}} \tag{36}$$

where $\mathbf{A}_i$ are 5×5 submatrices obtained by removing the i^{th} column of the 5×6 matrix in Eq. (35).

https://doi.org/10.1017/S0263574721001259 Published online by Cambridge University Press

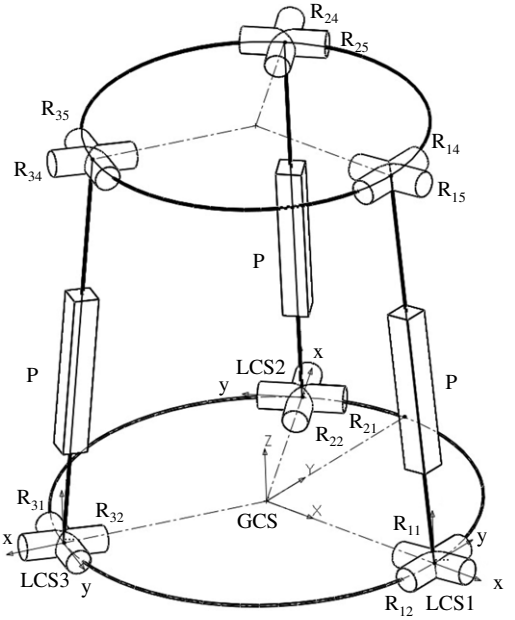


Figure 14. *$U_N^T - U_N^T$ PM.*

4. Instantaneous mobility analysis of 3-UPU PMs

We follow Zhao et al. [77] for the mobility analyses. In order to determine the DoF of PMs, first the limbs of the PMs are examined individually in their respective LCSs. The screws of the limbs are obtained according to the LCSs. The reciprocal screws of each limb are determined (Normalization is done if necessary). The reciprocal screws created for each limb are placed in a single matrix. Finally, the set of reciprocal screws are analyzed by singular value decomposition to obtain the DoF and the motion characteristics of the PM.

For a 3-UPU PM, each limb has a five-screw system. The reciprocal screws of the screws for each limb are then defined by Eq. (36). In general, three reciprocal screws are obtained for the 3-UPU PM. These screw sets are defined as

$$\$^r = \begin{bmatrix} \$_1^r \\ \$_2^r \\ \$_3^r \end{bmatrix} \tag{37}$$

Each of these screws represents a motion constraint on the platform. The set of reciprocal screws can be analyzed by singular value decomposition:

$$\$^r = \mathbf{USV}|\mathbf{A}_4|^{\mathrm{T}} \tag{38}$$

where $\mathbf{U}$ is an $m \times m$ orthogonal matrix, $\mathbf{V}$ is an $n \times n$ orthogonal matrix and $\mathbf{S}$ is an $m \times n$ diagonal matrix. The rows of $\mathbf{V}^{\mathrm{T}}$ corresponding to the zero singular values of an orthonormal basis of the null space of $\$^r$ and the remaining rows of $\mathbf{V}^{\mathrm{T}}$ form an orthonormal basis of the orthogonal complement. Therefore, the dimension of the constraint space of the PM is given by $d = \mathrm{Rank}\ (\$^r)$ and the DoF of the PM is given by $M = 6 - d$. In $\mathbf{V}^{\mathrm{T}}$ matrix, last M rows provide the motion characteristics of the PM.

The mobility analyses were performed for all 256 TNV-type PMs and 256 XYV-type PMs. The motion patterns of all PMs are listed in Appendix A. As an illustration of the procedure, the mobility analysis of a $\mathrm{U_N^T} - \mathrm{U_N^T}$ PM is presented here (Fig. 14). $\mathrm{R_{i1}}$ and $\mathrm{R_{i5}}$ joint axes of the first limb are along the x-axis of the LCS, whereas $\mathrm{R_{i1}}$ and $\mathrm{R_{i5}}$ joint axes of the second and third limbs are along the y-axis of the LCSs. From Tables II and III, limb type $\mathrm{k_6}$ is used for the first limb, whereas limb type $\mathrm{k_1}$ is used

https://doi.org/10.1017/S0263574721001259 Published online by Cambridge University Press

for the second and third limbs. The first limb of the PM is the R_x–R_x type. The second and third limbs are of R_y–R_y type. Using Table VII, the screw set for the first limb of the manipulator is found as

$$\begin{aligned}
\$_{11} &= (1, 0, 0; 0, 0, 0)\\
\$_{12} &= (0, 1, 0; 0, 0, 0)\\
\$_{13} &= (0, 0, 0; c\theta_1, 0, s\theta_1)\\
\$_{14} &= (0, 1, 0; \ -l_1 s\theta_1, 0, l_1 c\theta_1)\\
\$_{15} &= (1, 0, 0; 0, l_1 s\theta_1, 0)
\end{aligned} \tag{39}$$

The normalized reciprocal screw for the first limb is found as $\$_1^r = (0, 0, 0; 0, 0, s\theta_1)$. Using Table VI, the screw set for the second and third limbs of the manipulator are found as (for $i = 2, 3$)

$$\begin{aligned}
\$_{21} &= (0, 1, 0; 0, 0, 0)\\
\$_{22} &= (s\theta_i, 0, -c\theta_i; 0, 0, 0)\\
\$_{23} &= (0, 0, 0; c\theta_i, 0, s\theta_i)\\
\$_{24} &= (s\theta_i, 0, -c\theta_i; 0, l_i, 0)\\
\$_{25} &= (0, 1, 0; \ -l_i s\theta_i, 0, l_2 c\theta_i)
\end{aligned} \tag{40}$$

The normalized reciprocal screws for the second and third limbs are found as $\$_2^r = (0, 0, 0; c\theta_2, 0, s\theta_2)$ and $\$_3^r = (0, 0, 0; c\theta_3, 0, s\theta_3)$. In order to calculate the mobility of the PM, reciprocal screws calculated according to the LCS must be transformed into the GCS:

$$\begin{aligned}
\$_{G1}^r &= (0, 0, 0; 0, 0, 1)\\
\$_{G2}^r &= \left(0, 0, 0; \frac{1}{2}c\theta_2, \frac{-\sqrt{3}}{2}c\theta_2, s\theta_2\right)\\
\$_{G3}^r &= \left(0, 0, 0; \frac{1}{2}c\theta_3, \frac{\sqrt{3}}{2}c\theta_3, s\theta_3\right)
\end{aligned} \tag{41}$$

Since the all screws in Eq. (41) represent translations, the singularity analysis can be performed by looking at the determinant of the matrix composed of the secondary parts of the screws:

$$\begin{vmatrix} 0 & 0 & 1 \\ \frac{1}{2}c\theta_2 & \frac{-\sqrt{3}}{2}c\theta_2 & s\theta_2 \\ \frac{1}{2}c\theta_3 & \frac{\sqrt{3}}{2}c\theta_3 & s\theta_3 \end{vmatrix} = \frac{\sqrt{3}}{2}c\theta_2 c\theta_3 \tag{42}$$

So, the singular architectures of the PM are obtained for $\theta_2 = \theta_3 = 90^\circ$. That is, if the limbs are inclined with 90° in the initial configuration of the PM, the DoF of the PM is more than 3. When the limb angles of the PM are between 0° and 90°, the DoF of the PM is 3. For this PM, the reciprocal screws already imply the motion characteristics of the PM, but nevertheless let's check the last 3 rows of the $\mathbf{V}^{\mathrm{T}}$ matrix obtained by singular value decomposition of the matrix:

$$\mathbf{V}_\theta^{\mathrm{T}} = \begin{bmatrix} 0 & 0 & 0 & 0 & 0 & 1 \\ 0 & 0 & 0 & 0 & 1 & 0 \\ 0 & 0 & 0 & 1 & 0 & 0 \end{bmatrix} \tag{43}$$

Eq. (43) suggests that the PM is a TPM. The case where the limb angles of the PM are 90° in the initial configuration corresponds to the case of identical base and moving platforms. In this case from Eq. (41),

https://doi.org/10.1017/S0263574721001259 Published online by Cambridge University Press

all reciprocal screws are $\$^r_{Gi} = (0, 0, 0; 0, 0, 1)$ for $i = 1, 2, 3$, hence the PM has 5-DoF. Looking at the last five rows of the $\mathbf{V}^{\mathrm{T}}$ matrix obtained by singular value decomposition of the matrix:

$$\mathbf{V}^{\mathrm{T}}_{90^\circ} = \begin{bmatrix} 0 & 1 & 0 & 0 & 0 & 0 \\ 1 & 0 & 0 & 0 & 0 & 0 \\ 0 & 0 & 0 & 0 & 0 & 1 \\ 0 & 0 & 0 & 0 & 1 & 0 \\ 0 & 0 & 0 & 1 & 0 & 0 \end{bmatrix} \tag{44}$$

So, the PM can perform all translational motions and the rotational motions except rotation about the Z-axis.

For the XYV-type PMs, the limbs are along the z-axes of the LCSs, that is, $\theta = 90^\circ$, in the initial configuration of the PM. The mobility results for all classified PMs are presented in detail in Appendix A. Tables A.I–A.X list the PMs for which non-identical platforms are permissible. In these tables, the instantaneous mobility of the PMs may change according to whether the angles of the limbs are $\theta = 0^\circ$ or $0^\circ < \theta < 90^\circ$ at the initial configuration of the PM. The rotation DoF of the platform about the x-, y- and z-axes are, respectively, represented by $\mathrm{R_x}$, $\mathrm{R_y}$, $\mathrm{R_z}$, whereas the translation DoF are denoted by $\mathrm{T_x}$, $\mathrm{T_y}$, $\mathrm{T_z}$. When a twist involves more than one nonzero element in its six coordinates, it means that the twist represents a single-DoF motion with multiple rotation and/or translation components about/along different axis, that is, there is a parasitic motion. In the tables in Appendix A, the parasitic motions are represented in parenthesis. Each pair of parenthesis represents a single-DoF twist. For example, $(\mathrm{R_zT_y})$ means a twist with coordinates $(0, 0, a; 0, b, 0)$ with some nonzero, but coupled elements for $\mathrm{R_z}$ and $\mathrm{T_y}$ motions. The remaining tables starting from Table A.X consist only of PMs with identical base and moving platforms, and hence $\theta = 90^\circ$.

It should be noted that the results obtained provide the instantaneous mobility of the PMs in the initial configuration. The studies do not reflect the finite mobility information. A more through kinematic analysis should be performed in order to reveal the finite mobility characteristics of a specific PM. Raw motion analysis can be performed to check the finite mobility characteristics of the PMs, for example using the Motion module of SolidWorks [78]. As an example, for the $\mathrm{U^T_N} - \mathrm{U^T_N}$ PM with $\theta = 0^\circ \sim 90^\circ$ case with non-identical base and moving platforms, the moving platform has 3-DoF with $\mathrm{T_xT_yT_z}$-type motion (Table A.VIII). When raw motion analysis is performed with random inputs for the three prismatic joints, it is seen that the orientation of the moving platform does not change. Therefore, the moving platform has three translational finite DoF, that is, the PM is a TPM. For the $\theta = 90^\circ$ case, the instantaneous mobility of the PM in its initial configuration is found to be 5 with $\mathrm{R_xR_yT_xT_yT_z}$-type motion in Table A.XI. When the moving platform of the SolidWorks model of the PM is manually moved, it is seen that as oppose to the $\theta = 0^\circ \sim 90^\circ$ case, the PM is not a TPM anymore for the $\theta = 90^\circ$ case (Fig. 15a). The raw motion analysis in SolidWorks is started from a generic configuration where the moving platform is not parallel to the base platform. At this configuration, SolidWorks evaluates the instantaneous DoF as 3 (Fig. 15b). When raw motion analysis is performed in SolidWorks Motion with random inputs for the three prismatic joints, it is seen that both of the orientation and position of the moving platform changes. Although the moving platform has three DoF, all translational and rotational motions are observed due to parasitic motions.

The mobility characteristics of the 3-UPU PMs existing in the literature are verified in this study. Tsai's 3-UPU PM [4] is the $\mathrm{U^T}$–$\mathrm{U^T}$ PM in Table A.VIII, the SNU 3-UPU PM [9] is the $\mathrm{U^N}$–$\mathrm{U^N}$ PM in Table A.V, the parallel 3-UPU PMs [61] are the $\mathrm{U^X}$–$\mathrm{U^X}$ and $\mathrm{U^Y}$–$\mathrm{U^Y}$ PMs in Table A.XVIII, the vertical 3-UPU PM [57] are the $\mathrm{U^{VT}}$–$\mathrm{U^{VT}}$ PM in Table A.VI, Zhao's 3-UPU PM [64] is the $\mathrm{U^N}$–$\mathrm{U^{VT}}$ PM in Table A.XI, Lu and Hu's 3-UPU PM [65] is the $\mathrm{U^{VT}_N} - \mathrm{U^{VT}_N}$ PM in Table A.VIII, Hu and Lu's 3-UPU PM [67] is the $\mathrm{U^{VT}}$–$\mathrm{U^N}$ PM in Table A.X and Chebbi et al.'s [52] 3-UPU PMs are the $\mathrm{U^X_Y}$–$\mathrm{U^Y_X}$ PM in Table A.XVIII and $\mathrm{U^T_{VT}}$–$\mathrm{U^T_{VT}}$ PM in Table A.VIII.

https://doi.org/10.1017/S0263574721001259 Published online by Cambridge University Press

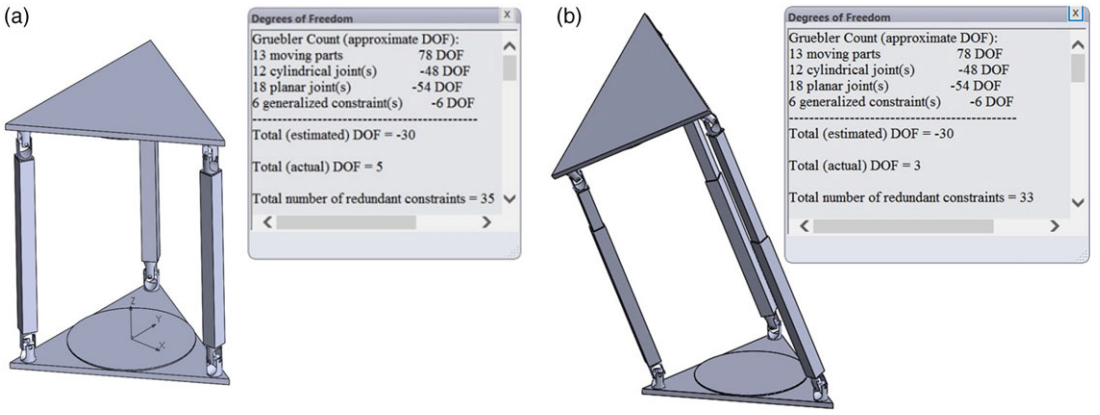


Figure 15. *(a) Result of SolidWorks Motion analysis of $U_N^T - U_N^T$ PM when $\theta = 90^\circ$ in parallel mode, (b) An arbitrary configuration for the SolidWorks Motion analysis of U_N^T-U_N^T PM when $\theta = 90^\circ$.*

Among the classified 3-UPU PMs, the 3-DoF PMs with non-parasitic motion may be considered to be valuable in applications. The DoF values in the tables in the Appendix A are instantaneous DoF values, however, if the instantaneous DoF is 3, it can be deduced that the finite DoF is also 3. The same conclusion cannot be drawn for the PMs with more than 3-DoF. Also, the instantaneous DoF being 3 is a necessary, but not sufficient condition to conclude that the finite DoF is 3.

The non-parasitic TPMs are only listed in Tables A.III and A.VIII and all these PMs are TNV-type PMs. Besides the Tsai 3-UPU PM [4], there are six types of novel TPMs: $U_{VT}^T - U_{VT}^T$, $U_T^{VT} - U_T^{VT}$ with $0^\circ < \theta < 90^\circ$, $U_N^T - U_N^T$, $U_N^{VT} - U_N^{VT}$ with $0^\circ \leq \theta < 90^\circ$ and $U_N^T - U_N^{VT}$, $U_N^{VT} - U_N^T$ with $\theta = 0^\circ$. Non-parasitic 3-DoF PMs with one rotational and two translation DoF are listed in Table A.XXIII with $R_xT_yT_z$ or $R_yT_xT_z$-type motion. All such PMs are XYV-type PMs, and there are 46 many of them. Non-parasitic 3-DoF PMs with two rotational and one translational (2R1T) DoF are listed in Tables A.V, A.XI, A.XVI, A.XXIII. Among the PMs listed in these tables, the PMs with $R_xR_zT_z$ motion in Table A.V are different from the others, because the PMs with $R_xR_zT_z$ motion has both rotational and translational DoF about the z-axis. There are six such novel PMs: $U_{VN}^T - U^{VN}$, $U_{VN}^T - U_T^{VN}$, $U_{VN}^T - U_N^{VN}$, $U_{VN}^N - U^{VN}$, $U_{VN}^N - U_T^{VN}$, $U_{VN}^N - U_N^{VN}$ with $\theta = 90^\circ$. The other PMs with 2R1T motion have $R_xR_yT_z$-type motion. Besides Zhao's $U^N - U^{VT}$ PM [64], there are 40 such novel PMs. Totally, 118 new 3-DoF non-parasitic 3-UPU PMs are found in this study.

5. Conclusions

In this study, different 3-UPU PM architectures are classified by considering possible joint layouts on the platforms, and the instantaneous mobility characteristics of 3-UPU PMs with equilateral platforms are investigated. Obtained 3-UPU PMs are tabulated according to their motion patterns. To the best knowledge of the authors, such a classification is performed for the first time in the literature. First, the topologies of the 3-UPU PMs available in the literature are examined and possible orientations of the U joint axes are determined. Various joint layouts are determined in accordance with the results obtained. Then, the joint layouts for the base and the moving platform are matched with each other. When these 3-UPU PM architectures are examined, it is found that they have similar limb structures. All studies are performed based on several assumptions listed in Section 2.2. The limbs are numerated and the kinematic properties of the limbs are examined using screw theory. The reciprocal screws of the limbs are derived in order to perform the instantaneous mobility analysis of PMs in their initial configurations. The results of the instantaneous mobility analysis are tabulated in order to give an insight into the future work of researchers. Also, the finite mobility analysis of one the PMs is performed using Solidworks Motion as an example.

https://doi.org/10.1017/S0263574721001259 Published online by Cambridge University Press

Among the classified PMs, 118 of them are novel 3-DoF 3-UPU PMs with non-parasitic motion: 6 TPMs, 46 PMs with 1 rotational and 2 translational DoF, 6 PMs with $R_xR_zT_z$ and 40 PMs with $R_xR_yT_z$-type motion. These non-parasitic PMs have potential use in industrial applications.

Acknowledgments. Contributions of Prof. M. İ. Can Dede and Prof. Erkin Gezgin are gratefully acknowledged.

Author Contributions. G. Kiper defined the problem; S. Boztaş came up with the assumptions and they applied the methodology together.

Financial Support. This research received no specific grant from any funding agency, commercial or not-for-profit sectors.

Competing interests. The authors declare none.

References

[1] X. S. Gao, D. Lei, Q. Liao and G. F. Zhang, "Generalized Stewart-Gough platforms and their direct kinematics," *IEEE Trans. Robot.* **21**, 141–151 (2005).
[2] M. Toz and S. Kucuk, "Dimensional optimization of 6-DOF 3-CCC type asymmetric parallel manipulator," *Adv. Robot.* **28**(9), 625–637 (2014).
[3] M. Toz and S. Kucuk, "Dexterous workspace optimization of an asymmetric six-degree of freedom Stewart–Gough platform type manipulator," *Rob. Auton. Syst.* **61**, 1516–1528 (2013).
[4] L.-W. Tsai, "Kinematics of a Three-Dof Platform with Three Extensible Limbs," In: *Recent Advances in Robot Kinematics*. (Kluwer Academic Publisher, 1996) pp. 401–410.
[5] L. Yi, "Computer-aided geometric machining of a 3D free surface using a 3-UPU spatial parallel machine tool," *Int. J. Adv. Manuf. Tech.* 26(9–10), 1018–1025 (2005).
[6] Z. Qi, H. Wang, Z. Huang and L. Zhang, "Kinematics of a Quadruped/Biped Reconfigurable Walking Robot with Parallel Leg Mechanisms," *Proceedings ASME/IFToMM Int. Conf Reconfigurable Mechanisms and Robots*, London (2009) pp. 558–564.
[7] S. Li, A. Frisoli, M. Solazzi and M. Bergamasco, "Mechanical Design and Optimization of a Novel fMRI Compatible Haptic Manipulator," *Proceedings 19th Int. Symp. Robot and Human Interactive Communication*, Viareggio, Italy (2010) pp. 1–6.
[8] M. Dehkordi, A. Frisoli, E. Sotgiu and M. Bergamasco, "Modelling and experimental evaluation of a static balancing technique for a new horizontally mounted 3-UPU parallel mechanism," *Int. J. Adv. Robotic Sy.* **9**(5), 193 (2012).
[9] C. Han, J., Kim, J. Kim and F. C. Park, "Kinematic sensitivity analysis of the 3-UPU parallel mechanism," *Mech. Mach. Theory* **37**(8), 787–798 (2002).
[10] A. Wolf and M. Shoham, "Investigation of parallel manipulators using linear complex approximation," *ASME J. Mech. Des.* **125**(3), 564–572 (2003).
[11] G. Liu, Y. Lou and Z. Li, "Singularities of parallel manipulators: a geometric treatment," *IEEE Trans,* Robot, Autom. **19**(4), 579–594 (2003).
[12] D. R. Walter, M. L. Husty and M. Pfurner, "The SNU 3-UPU parallel robot from a theoretical viewpoint," *Proceedings* 2nd *Int. Workshop on Fundamental Issues and Future Research Directions for Parallel Mechanisms and Manipulators*, Montpellier, France (2008).
[13] G. Gogu (2008) "Constraint Singularities and the Structural Parameters of Parallel Robots," *Advances in Robot Kinematics: Analysis and Design* (Springer, 2008) pp. 21–28.
[14] H. Qu, Y. Fang and S. Guo, "Parasitic rotation evaluation and avoidance of 3-UPU parallel mechanism," *Front. Mech. Eng.* **7**(2), 210–218, 2012.
[15] I. Bonev and D. Zlatanov D, *The Mystery of the Singular SNU Translational Parallel Robot*. ParalleMIC-The Parallel Mechanisms Information Center, Report no 4, 2001.
[16] A. Wolf, M. Shoham and F. C. Park, "Investigation of Singularities and Self-Motions of the 3-UPU Robot," *Advances in Robot Kinematics* (Springer, 2002) pp. 165–174.
[17] D. Zlatanov, I. Bonev and C. Gosselin, "Constraint Singularities of Parallel Mechanisms," *Proceedings 2002 IEEE Int. Conf. Robotics and Automation*, Washington, DC (2002) pp. 496–502.
[18] S. Li and Z. Huang, "Instantaneous Kinematic Characteristics of a Special 3-UPU Parallel Manipulator," *Proceedings ASME 29th Mechanisms and Robotics Conf.*, Long Beach, CA (2005) pp. 691–697.
[19] Z. Chen, Y. Zhang, K. Huang and Z. Huang, "Constraint and Mobility Analysis of the SNU 3-UPU Parallel Mechanism in Mixed Mode," *Advances in Reconfigurable Mechanisms and Robots II*, Springer (2016) pp. 385–394.
[20] A. Wolf and M. Shoham, "Screw theory tools for the synthesis of the geometry of a parallel robot for a given instantaneous task," *Mech. Mach. Theory* **41**(6), 656–670 (2006).
[21] Z. Chen, Y. Zhang, K. Huang, H. Ding and Z. Huang, "Mobility and Motion Analysis of a Special 3-UPU Parallel Mechanism," *Proceedings 14th IFToMM World Congress*, Taipei, ROC, vol. 4 (2015) pp. 256–263.
[22] L.-W. Tsai and S. Joshi, "Kinematics and optimization of a spatial 3-UPU parallel manipulator," *ASME J. Mech. Des.* **122**(4), 439–446 (2000).

https://doi.org/10.1017/S0263574721001259 Published online by Cambridge University Press

[23] L.-W. Tsai and S. Joshi, "Comparison Study of Architectures of Four 3 Degree-of-Freedom Translational Parallel Manipulators," *Proceedings 2001 IEEE Int. Conf. Robotics and Automation*, Seoul, South Korea, vol. 2 (2001) pp. 1283–1288.

[24] S. Joshi and L.-W. Tsai, "Jacobian analysis of limited-dof parallel manipulators," *ASME J. Mech. Des*, **124**(2), 254–258, 2002.

[25] V. Parenti-Castelli, R. Di Gregorio and F. Bubani, "Workspace and optimal design of a pure translation parallel manipulator," *Meccanica* **35**, 203–214 (2000).

[26] D. Kanaan, P. Wenger and D. Chablat, "Singularity Analysis of Limited-Dof Parallel Manipulators Using Grassmann-Cayley Algebra," *Advances in Robot Kinematics: Analysis and Design* (Springer, 2008) pp. 59–68.

[27] D. Kanaan, P. Wenger, S. Caro and D. Chablat, "Singularity analysis of lower mobility parallel manipulators using Grassmann–Cayley algebra," *IEEE Trans. Robot*. **25**(5), 995–1004 (2009).

[28] Y. Yang and J. F. O'Brien, "A Geometric Approach for the Design of Singularity-Free Parallel Robots," *Proceedings 2009 IEEE Int. Conf. Robotics and Automation*, Kobe, Japan (2009) pp. 1801–1806.

[29] S. Joshi and L.-W. Tsai, "A comparison study of two 3-DOF parallel manipulators: One with three and the other with four supporting legs," *IEEE Trans. Robot. Autom.* **19**(2), 200–209 (2003).

[30] R. Di Gregorio and V. Parenti-Castelli, "Mobility analysis of the 3-UPU parallel mechanism assembled for a pure translational motion," *ASME J. Mech. Des.* **124**(2), 259–264 (2002).

[31] J.-S. Zhao, Z.-J. Feng and J.-X. Dong, "Computation of the configuration degree of freedom of a spatial parallel mechanism by using reciprocal screw theory," *Mech. Mach. Theory* **41**(12), 1486–1504 (2006).

[32] R. Di Gregorio and V. Parenti-Castelli, "A New Approach for the Evaluation of Kinematic and Static Performances of a Family of 3-UPU Translational Manipulators," *Romansy 16* (Springer, 2006) pp. 47–54.

[33] D. R. Walter and M. Husty, "Kinematic Analysis of the Tsai-3UPU Parallel Manipulator Using Algebraic Methods," *Proceedings 13th World Congress in Mechanism and Machine Science*, Guanajuato, Mexico (2011) pp. 19–25.

[34] Y. Yang and J. F. O'Brien, "Singularity-Free Workspace Design for the Translational 3-UPU Parallel Robot," *2010 IEEE Int. Conf. Automation Science and Engineering*, Toronto, Canada (2010) pp. 222–227.

[35] J. Bałchanowski, "Some aspects of topology and kinematics of a 3DOF translational parallel mechanism," *Int. J. Appl. Mech. Eng.* **19**(1), 5–15 (2014).

[36] L.-W. Guan, J.-S. Wang and L.-P. Wang, "Mobility Analysis of the 3-UPU Parallel Mechanism Based on Screw Theory," *Proceedings 2004 IEEE Int. Conf. Intelligent Mechatronics and Automation*, Chengdu, PRC (2004) pp. 309–314.

[37] J.-S. Zhao, Z.-J. Feng, K. Zhou and J.-X. Dong, "Analysis of the singularity of spatial parallel manipulator with terminal constraints," *Mech. Mach. Theory* **40**(3), 275–284 (2005).

[38] M. Badescu and C. Mavroidis, "Workspace optimization of 3-legged UPU and UPS parallel platforms with joint constraints," *ASME J. Mech. Des.* **126**(2), 291–300 (2004).

[39] A. Chebbi, Z. Affi and L. Romdhane, "Prediction of the pose errors produced by joints clearance for a 3-UPU parallel robot," *Mech. Mach. Theory* **44**(9), 1768–1783 (2009).

[40] J. Bi and R. Wen, (2010) Errors Analysis of 3-UPU Parallel Manipulator Using Screw Theory," *Proceeding Int. Conf. Measuring Technology and Mechatronics Automation*, Changsha, PRC (2010) pp. 137–140.

[41] N. Wang, S. Guo, Y. Fang and X. Li, "Error Sensibility Analysis of 3-UPU Parallel Manipulator Based on Probability Distribution," *Proceedings* 2nd *Int. Conf. Mechanic Automation and Control Engineering*, Hohhot, PRC (2011) pp. 1296–1301.

[42] S. H. Sun, "Accuracy analysis of 3-UPU translational parallel robot mechanism," *Adv. Mat. Res.* **694–697**, 1617–1620 (2013).

[43] G. Bhutani and T. Dwarakanath, "Novel design solution to high precision 3 axes translational parallel mechanism," *Mech. Mach. Theory* **75**, 118–130 (2014).

[44] C. Guohua, W. Bin, W. Nan and Z. Yanwei, "Stiffness, workspace analysis and optimization for 3UPU parallel robot mechanism," *Indones. J. Electrical Eng. Comput. Sci.* **11**(9), 5253–5261 (2013).

[45] B. Aboulissane and L. El Bakkali, "Modeling and simulation of spatial mechanism," *Proceedings Xth Int. Conf. Integrated Design and Production*, Tangier, Morocco (2015).

[46] M. Laribi, A. Mlika, L. Romdhane and S. Zeghloul, "Geometric and Kinematic Performance Analysis and Comparison of Three Translational Parallel Manipulators," *Proceedings 14th IFToMM World Congress*, Taipei, ROC, vol. 2 (2015) pp. 565–571.

[47] Y. Wei, Y. Fan, Q. Li and Z. Wang, "Structure optimization design of 3-UPU parallel mechanism based on the comprehensive dexterity." *Recent Adv. Electr. Electron. Eng.* **8**(1), 26–32 (2015).

[48] M. Karouia and J. Hervé, "A Three-Dof Tripod for Generating Spherical Rotation," *Advances in Robot Kinematics* (Springer, 2000) pp. 395–402.

[49] R. Di Gregorio, "Kinematics of the 3-UPU wrist," *Mech. Mach. Theory* **38**(3), 253–263 (2003).

[50] R. Di Gregorio, "Statics and singularity loci of the 3-UPU wrist," *IEEE Trans. Robot.* **20**, 630–635 (2004).

[51] D. Paganelli, "Avoiding Parallel Singularities of 3UPS and 3UPU Spherical Wrists," *Proceedings 2007 IEEE Int. Conf. Robotics and Automation*, Rome, Italy (2007) pp. 1201–1206.

[52] A. Chebbi, Z. Affi and L. Romdhane, "Modelling and analysis of the 3-UPU spherical manipulator," *Eur. J. Comput. Mech.* **22**(2–4), 157–169 (2013).

[53] S. Pramanik and A. Ghosal, "Development of a sun tracking system using a 3-UPU spherical wrist manipulator," *Proceedings 2nd Int. and 17th Nati Conf. Machines and Mechanisms*, Kanpur, India (2015).

https://doi.org/10.1017/S0263574721001259 Published online by Cambridge University Press

[54] Z. Xiangzhou, B. Hongzan and L. Yougao, "Kinematics of 3-UPU parallel manipulator with a pure spherical motion based on quaternion transformation," *Adv. Syst. Sci. Appl.* **6**(2), 334–340 (2006).
[55] Z. Xiangzhou, L. Yougao and B. Hongzan, "Inverse Dynamics of 3-UPU Parallel Mechanism with Pure Rotation Based on D'Alembert Principle," *Proceedings 2007 IEEE Int. Conf. Mechatronics and Automation*, Harbin, PRC (2007) pp. 2842–2847.
[56] R. B. Ashith Shyam and A. Ghosal, "Path planning of a 3-UPU wrist manipulator for sun tracking in central receiver tower systems," *Mech. Mach. Theory* **119**, 130–141 (2018).
[57] Z. Huang and Q. Li, "Construction and Kinematic Properties of 3-UPU Parallel Mechanisms," *Proceedings ASME 27th Biennial Mechanisms and Robotics Conf.*, Montreal, Canada (2002) pp. 1027–1033.
[58] G. Kiper and E. Söylemez E, "Kinematic Analysis of a 3-UPU Parallel Manipulator Using Exponential Rotation Matrices," *Machines and Mechanisms*, Narosa, New Delhi, India (2012) pp. 123–131.
[59] S. Guo, N. Wang, Y. Fang and X. Li, "Study on Error Sensibility of UPU Parallel Manipulator Based on Probability Distribution," *Proceedings 2011 IEEE Int. Conf. Mechatronics and Automation*, Beijing, PRC (2011) pp. 2045–2050.
[60] Z. Huang, S. Li and R. Zuo, "Feasible instantaneous motions and kinematic characteristics of a special 3-dof 3-UPU parallel manipulator," *Mech. Mach. Theory* **39**(9), 957–970 (2004).
[61] J. Yu, J. Dai, T. Zhao, S. Bi and G. Zong, "Mobility analysis of complex joints by means of screw theory," *Robotica* **27**(6), 915–927 (2009).
[62] P. Binbin, L. Zengming, W. Kai and S. Yu, "Kinematic characteristics of 3-UPU parallel manipulator in singularity and its application," *Int. J. Adv. Robot. Syst.* **8**(4), 54–64 (2011).
[63] Z. Miao, Y. Yao and X. Kong, "A rolling 3-UPU parallel mechanism," *Front. Mech. Eng.* **8**, 340–349 (2013).
[64] J.-S. Zhao, Z.-J. Feng, K. Zhou and D.-W. Jin, "Re-analysis of the degree-of-freedom configuration of the platforms in spatial parallel mechanisms with constraints spaces," *Int. J. Adv. Manuf. Technol.* 28, 190–196 (2006).
[65] Y. Lu and B. Hu, "Analysis of kinematics and solution of active/constrained forces of asymmetric 2UPU+X parallel manipulators," *Proc. Inst. Mech. Eng. C J. Mech. Eng. Sci.* 220(12), 1819–1830 (2006).
[66] Y. Lu, Y. Shi and B. Hu, "Kinematic analysis of two novel 3UPU I and 3UPU II PKMs," *Robot. Auton. Syst.* **56**(4), 296–305 (2008).
[67] B. Hu and Y. Lu, "Solving stiffness and deformation of a 3-UPU parallel manipulator with one translation and two rotations," *Robotica* **29**(6), 815–822 (2011).
[68] A. Chebbi and V. Parenti-Castelli, "Potential of the 3-UPU Translational Parallel Manipulator," *Proceedings ASME 34th Annual Mechanisms and Robotics Conf.*, Montreal, Canada (2010) pp. 1089–1099.
[69] M. Wang and M. Ceccarelli, "Design and simulation for kinematic characteristics of a tripod mechanism for biped robots," *Int. J. Mech. Control* **15**(1), 11–18 (2013).
[70] M. Wang, G. Carbone and M. Ceccarelli, "Stiffness analysis for a tripod leg mechanism," *Proceedings 14th IFToMM World Congress*, Taipei, ROC, vol. 2 (2015).
[71] M. Wang, M. Ceccarelli and G. Carbone, "A feasibility study on the design and walking operation of a biped locomotor via dynamic simulation," *Front. Mech. Eng.* **11**(2), 144–158 (2016).
[72] M. Wang, M. Ceccarelli and G. Carbone, "Design and development of the Cassino biped locomotor," ASME *J. Mech. Robot.* **12**(3), 031001 (2020).
[73] S. Sarabandi, P. Grosch, J. M. Porta and F. Thomas, "A Reconfigurable Asymmetric 3-UPU Parallel Robot," *Proceedings 2018 Int. Conf. Reconfigurable Mechanisms and Robots*, Delft, Netherlands (2018) pp. 404–410.
[74] C. Zhao, Z. Chen, Y. Li and Z. Huang, "Motion characteristics analysis of a novel 2R1T 3-UPU parallel mechanism," *ASM. J. Mech. Des.*, **142**(1), 012302, 2020.
[75] R. Di Gregorio, "A review of the literature on the lower-mobility parallel manipulators of 3-UPU or 3-URU type," *Robotics*, **9**(1), 5 (2020).
[76] J. Dai and J. Jones, "A linear algebraic procedure in obtaining reciprocal screw systems," *J. Robotic Syst.* **20**, 401–412 (2003).
[77] J.-S. Zhao, Z.-J. Feng, F. Chu and N. Ma, *Advanced Theory of Constraint and Motion Analysis for Robot Mechanisms* (Academic Press, 2013).
[78] E. Gezgin, *Biokinematic Analysis of Human Arm*, İzmir Institute of Technology MSc Thesis (2006).

APPENDIX A

Table A.I. *Mobility properties of TNV-type PMs with 5-DoF for $\theta = 0^\circ$*

$\mathbf{R_x R_y T_x T_y T_z}$
$U^N - U^N$

https://doi.org/10.1017/S0263574721001259 Published online by Cambridge University Press

Table A.II. *Mobility properties of TNV-type PMs with 4-DoF for $\theta = 0°$*

$\mathbf{R_xR_yT_xT_z}$	$\mathbf{R_yT_xT_yT_z}$
$U^N - U^N_{VT}$, $U^N_{VT} - U^N$, $U^N - U^N_T$, $U^N_T - U^N$	$U^N_T - U^N_T$, $U^N_{VT} - U^N_{VT}$, $U^N_T - U^N_{VT}$, $U^N_{VT} - U^N_T$

$\mathbf{R_zT_xT_yT_z}$
$U^T - U^T$, $U^T_{VT} - U^T_{VT}$, $U^{VT}_T - U^{VT}_T$, $U^T - U^T_{VT}$, $U^T_{VT} - U^T$, $U^{VT} - U^{VT}_T$, $U^{VT}_T - U^{VT}$, $U^T - U^{VT}$, $U^T - U^{VT}_T$, $U^T_{VT} - U^{VT}_T$, $U^{VT} - U^T$, $U^{VT}_T - U^T_{VT}$, $U^{VT}_T - U^T$, $U^T_{VT} - U^{VT}$, $U^{VT} - U_{VT}$

Table A.III. *Mobility properties of TNV-type PMs with 3-DoF for $\theta = 0°$*

$\mathbf{T_xT_yT_z}$
$U^T_N - U^T_N$, $U^{VT}_N - U^{VT}_N$, $U^T_N - U^{VT}_N$, $U^{VT}_N - U^T_N$

$\mathbf{R_xR_yT_z}$
$U^N - U^T$, $U^N - U^T_{VT}$, $U^N - U^{VT}$, $U^N - U^{VT}_T$, $U^N - U^{VT}_N$, $U^N_T - U^T_N$, $U^N_{VT} - U^T_N$, $U^N_T - U^{VT}_N$, $U^N_{VT} - U^{VT}_N$, $U^T - U^N$, $U^T_N - U^N_T$, $U^T_N - U^N_{VT}$, $U^T_{VT} - U^N$, $U^{VT} - U^N$, $U^{VT}_N - U^N_{VT}$, $U^{VT}_T - U^N$, $U^{VT}_N - U^N_T$ $U^{VT}_N - U^N$, $U^N - U^T_N$, $U^T_N - U^N$

Table A.IV. *Mobility properties of TNV-type PMs with 3-DoF with one parasitic mobility for $\theta = 0°$*

$\mathbf{R_yT_z(R_zT_xT_y)}$
$U^N_T - U^T$, $U^N_T - U^T_{VT}$, $U^N_{VT} - U^T$, $U^N_T - U^{VT}$, $U^N_T - U^{VT}_T$, $U^N_{VT} - U^{VT}_T$, $U^N_{VT} - U^T_{VT}$, $U^N_{VT} - U^{VT}$

$\mathbf{R_yT_z(R_zT_y)}$
$U^T - U^N_T$, $U^T - U^N_{VT}$, $U^T_{VT} - U^N_T$, $U^{VT} - U^N_T$, $U^{VT}_T - U^N_{VT}$, $U^{VT}_T - U^N_T$, $U^T_{VT} - U^N_{VT}$, $U^{VT} - U^N_{VT}$

$\mathbf{T_xT_z(R_zT_y)}$
$U^T - U^T_N$, $U^T_N - U^T$, $U^T_N - U^T_{VT}$, $U^T_{VT} - U^T_N$, $U^{VT} - U^{VT}_N$, $U^{VT}_N - U^{VT}$, $U^{VT}_T - U^{VT}_N$, $U^{VT}_N - U^{VT}_T$, $U^T - U^{VT}_N$, $U^T_N - U^{VT}$, $U^T_N - U^{VT}_T$, $U^T_{VT} - U^{VT}_N$, $U^{VT} - U^T_N$, $U^{VT}_N - U^T_{VT}$, $U^{VT}_T - U^T_N$, $U^{VT}_N - U^T$

Table A.V. *Mobility properties of TNV-type PMs with 5-DoF for $0° < \theta < 90°$*

$\mathbf{R_xR_yT_xT_yT_z}$
$U^N - U^N$

Table A.VI. *Mobility properties of TNV-type PMs with 4-DoF for $0° < \theta < 90°$*

$\mathbf{R_xR_yT_xT_z}$	$\mathbf{R_yT_xT_yT_z}$	$\mathbf{R_zT_xT_yT_z}$
$U^N - U^N_T$, $U^N - U^N_{VT}$	$U^N_T - U^N_T$, $U^N_{VT} - U^N_{VT}$	$U^{VT} - U^{VT}$

https://doi.org/10.1017/S0263574721001259 Published online by Cambridge University Press

Table A.VII. *Mobility properties of TNV-type PMs with 4-DoF with one parasitic mobility for $0^\circ < \theta < 90^\circ$*

$\mathbf{R_yT_xT_z(R_xT_y)}$
$U^N_T - U^N,\ U^N_T - U^N_{VT},\ U^N_{VT} - U^N,\ U^N_{VT} - U^N_T$

Table A.VIII. *Mobility properties of TNV-type PMs with 3-DoF for $0^\circ < \theta < 90^\circ$*

$\mathbf{T_xT_yT_z}$	$\mathbf{R_xR_yT_z}$
$U^T - U^T,\ U^T_N - U^T_N,\ U^T_{VT} - U^T_{VT},$ $U^{VT}_T - U^{VT}_T,\ U^{VT}_N - U^{VT}_N$	$U^N - U^T,\ U^N - U^T_N,\ U^N - U^T_{VT},\ U^N - U^{VT},$ $U^N - U^{VT}_T,\ U^N - U^{VT}_T$

Table A.IX. *Mobility properties of TNV-type PMs with 3-DoF with one parasitic mobility for $0^\circ < \theta < 90^\circ$*

$\mathbf{R_yT_z(R_xR_zT_xT_y)}$
$U^N_T - U^T,\ U^N_T - U^T_N,\ U^N_T - U^T_{VT},\ U^N_{VT} - U^T,\ U^N_{VT} - U^T_N,\ U^N_T - U^{VT},\ U^N_T - U^{VT}_T,\ U^N_T - U^{VT}_N,$ $U^N_{VT} - U^{VT}_T,\ U^N_{VT} - U^{VT}_T$

$\mathbf{R_yT_z(R_zT_xT_y)}$	$\mathbf{T_xT_z(R_xR_zT_y)}$
$U^N_{VT} - U^T_{VT},\ U^N_{VT} - U^{VT}$	$U^T - U^T_N,\ U^T_N - U^T,\ U^T - U^T_{VT},\ U^T_N - U^T_{VT},\ U^T_{VT} - U^T,\ U^T_{VT} - U^T_N$

$\mathbf{T_xT_z(R_zT_y)}$
$U^{VT} - U^{VT}_T,\ U^{VT} - U^{VT}_N,\ U^{VT}_T - U^{VT},\ U^{VT}_N - U^{VT},\ U^{VT}_T - U^{VT}_N,\ U^{VT}_N - U^{VT}_T$

Table A.X. *Mobility properties of TNV-type PMs with 3-DoF with two parasitic mobility for $0^\circ < \theta < 90^\circ$*

$\mathbf{T_z(R_xR_yR_zT_xT_y)(R_xR_zT_xT_y)}$
$U^T - U^N,\ U^T - U^N_T,\ U^T_N - U^N_T,\ U^T - U^N_{VT},\ U^T_N - U^N_{VT},\ U^T_{VT} - U^N,\ U^T_{VT} - U^N_T,\ U^T - U^{VT},\ U^T - U^{VT}_T$ $U^T - U^{VT}_N,\ U^T_N - U^{VT},\ U^T_N - U^{VT}_T,\ U^T_{VT} - U^{VT}_T,\ U^T_{VT} - U^{VT}_N,\ U^{VT} - U^T,\ U^{VT} - U^N,\ U^{VT} - U^T_N,$ $U^{VT} - U^N_T,\ U^{VT}_T - U^T_{VT},\ U^{VT}_T - U^N_{VT},\ U^{VT}_N - U^T_{VT},\ U^{VT}_N - U^N_{VT},\ U^{VT}_T - U^T,\ U^{VT}_T - U^N,\ U^{VT}_T - U^T_N,$ $U^{VT}_T - U^N_T,\ U^{VT}_N - U^T,\ U^{VT}_N - U^T_N,$

$\mathbf{T_z(R_xR_yR_zT_xT_y)(R_yT_xT_y)}$	$\mathbf{T_z(R_yR_zT_xT_y)(R_zT_xT_y)}$	$\mathbf{T_z(R_yR_zT_xT_y)(R_zT_y)}$
$U^T_N - U^N,\ U^T_N - U^{VT}_N,\ U^{VT}_N - U^N,\ U^{VT}_N - U^T_N$	$U^T_{VT} - U^N_{VT},\ U^T_{VT} - U^{VT}$	$U^{VT} - U^T_{VT},\ U^{VT} - U^N_{VT}$

https://doi.org/10.1017/S0263574721001259 Published online by Cambridge University Press

Table A.XI. *Mobility properties of TNV-type PMs with 5-DoF for $\theta = 90°$*

$\mathbf{R_xR_yT_xT_yT_z}$
$U^T - U^T$, $U^T - U^N$, $U^T - U^T_N$, $U^T - U^N_T$, $U^N - U^T$, $U^N - U^N$, $U^N - U^T_N$, $U^N - U^N_T$, $U^T_N - U^T$, $U^T_N - U^N$, $U^T_N - U^T_N$, $U^T_N - U^N_T$, $U^N_T - U^T$, $U^N_T - U^N$, $U^N_T - U^T_N$, $U^N_T - U^N_T$

Table A.XII. *Mobility properties of TNV-type PMs with 4-DoF for $\theta = 90°$*

$\mathbf{R_xR_yR_zT_z}$
$U^T - U^{VN}$, $U^N - U^{VN}$, $U^T_N - U^{VN}$, $U^N_T - U^{VN}$
$\mathbf{R_xR_yT_xT_z}$
$U^T - U^T_{VT}$, $U^T - U^N_{VT}$, $U^N - U^T_{VT}$, $U^N - U^N_{VT}$, $U^T_N - U^T_{VT}$, $U^T_N - U^N_{VT}$, $U^N_T - U^T_{VT}$, $U^N_T - U^N_{VT}$
$\mathbf{R_xR_yT_yT_z}$
$U^T - U^T_{VN}$, $U^T - U^N_{VN}$, $U^N - U^T_{VN}$, $U^N - U^N_{VN}$, $U^T_N - U^T_{VN}$, $U^T_N - U^N_{VN}$, $U^N_T - U^T_{VN}$, $U^N_T - U^N_{VN}$

Table A.XIII. *Mobility properties of TNV-type PMs with 4-DoF with one parasitic mobility for $\theta = 90°$*

$\mathbf{R_xR_yT_z(R_zT_y)}$	
$U^T - U^{VT}_{VN}$, $U^N - U^{VT}_{VN}$, $U^T_N - U^{VT}_{VN}$, $U^N_T - U^{VT}_{VN}$	
$\mathbf{R_xT_yT_z(R_yT_x)}$	**$\mathbf{R_yT_xT_z(R_xT_y)}$**
$U^T_{VN} - U^T$, $U^T_{VN} - U^N$, $U^T_{VN} - U^T_N$, $U^T_{VN} - U^N_T$, $U^T_{VN} - U^T_{VN}$, $U^T_{VN} - U^N_{VN}$, $U^N_{VN} - U^T$, $U^N_{VN} - U^N$, $U^N_{VN} - U^T_N$, $U^N_{VN} - U^N_T$, $U^N_{VN} - U^T_{VN}$, $U^N_{VN} - U^N_{VN}$	$U^T_{VT} - U^T$, $U^T_{VT} - U^N$, $U^T_{VT} - U^T_N$, $U^T_{VT} - U^N_T$, $U^T_{VT} - U^T_{VT}$, $U^T_{VT} - U^N_{VT}$, $U^N_{VT} - U^T$, $U^N_{VT} - U^N$, $U^N_{VT} - U^T_N$, $U^N_{VT} - U^N_T$, $U^N_{VT} - U^T_{VT}$, $U^N_{VT} - U^N_{VT}$

Table A.XIV. *Mobility properties of TNV-type PMs with 4-DoF with two parasitic mobility for $\theta = 90°$*

$\mathbf{R_xT_z(R_yT_xT_y)(R_yT_x)}$	$\mathbf{R_yT_z(R_xT_xT_y)(R_xT_x)}$	$\mathbf{R_zT_z(R_xT_y)(R_yT_x)}$
$U^T_{VN} - U^T_{VT}$, $U^T_{VN} - U^N_{VT}$, $U^N_{VN} - U^T_{VT}$, $U^N_{VN} - U^N_{VT}$	$U^T_{VT} - U^T_{VN}$, $U^T_{VT} - U^N_{VN}$, $U^N_{VT} - U^T_{VN}$, $U^N_{VT} - U^N_{VN}$	$U^{VN} - U^{VN}$

Table A.XV. *Mobility properties of TNV-type PMs with 3-DoF for $\theta = 90°$*

$\mathbf{R_xR_yT_z}$	$\mathbf{R_xR_zT_z}$
$U^T - U^{VT}$, $U^T - U^{VT}_T$, $U^T - U^{VN}_T$, $U^T - U^{VT}_N$, $U^T - U^{VN}_N$, $U^T - U^{VN}_{VT}$, $U^N - U^{VT}$, $U^N - U^{VT}_T$, $U^N - U^{VN}_T$, $U^N - U^{VT}_N$, $U^N - U^{VN}_N$, $U^N - U^{VN}_{VT}$, $U^T_N - U^{VT}$, $U^T_N - U^{VT}_T$, $U^T_N - U^{VN}_T$, $U^T_N - U^{VT}_N$, $U^T_N - U^{VN}_N$, $U^T_N - U^{VN}_{VT}$, $U^N_T - U^{VT}$, $U^N_T - U^{VT}_T$, $U^N_T - U^{VN}_T$, $U^N_T - U^{VT}_N$, $U^N_T - U^{VN}_N$, $U^N_T - U^{VN}_{VT}$	$U^T_{VN} - U^{VN}$, $U^T_{VN} - U^{VN}_T$, $U^T_{VN} - U^{VN}_N$, $U^N_{VN} - U^{VN}$, $U^N_{VN} - U^{VN}_T$, $U^N_{VN} - U^{VN}_N$

https://doi.org/10.1017/S0263574721001259 Published online by Cambridge University Press

Table A.XVI. *Mobility properties of TNV-type PMs with 3-DoF with one parasitic mobility for* $\theta = 90^\circ$

$\mathbf{R_xT_z(R_yR_z)}$	$\mathbf{R_xT_z(R_yR_zT_y)}$	$\mathbf{R_xT_z(R_zT_y)}$
$U^T_{VN} - U^{VN}_{VT}$, $U^N_{VN} - U^{VN}_{VT}$	$U^T_{VN} - U^{VT}$, $U^N_{VN} - U^{VT}$	$U^T_{VN} - U^{VT}_T$, $U^T_{VN} - U^{VT}_{VN}$, $U^N_{VN} - U^{VT}_T$, $U^N_{VN} - U^{VT}_N$, $U^N_{VN} - U^{VT}_{VN}$, $U^T_{VN} - U^{VT}_N$

$\mathbf{R_yT_z(R_xR_z)}$	$\mathbf{R_yT_z(R_xR_zT_y)}$
$U^T_{VT} - U^{VN}$, $U^T_{VT} - U^{VN}_T$, $U^T_{VT} - U^{VN}_N$, $U^T_{VT} - U^{VN}_{VT}$, $U^N_{VT} - U^{VN}$, $U^N_{VT} - U^{VN}_T$, $U^N_{VT} - U^{VN}_N$, $U^N_{VT} - U^{VN}_{VT}$	$U^T_{VT} - U^{VT}$, $U^T_{VT} - U^{VT}_T$, $U^T_{VT} - U^{VT}_N$, $U^T_{VT} - U^{VT}_{VN}$, $U^N_{VT} - U^{VT}$, $U^N_{VT} - U^{VT}_T$, $U^N_{VT} - U^{VT}_N$, $U^N_{VT} - U^{VT}_{VN}$

$\mathbf{R_zT_z(R_xR_yT_xT_y)}$
$U^{VN} - U^T$, $U^{VN} - U^N$, $U^{VN} - U^T_N$, $U^{VN} - U^N_T$, $U^{VN} - U^T_{VN}$, $U^{VN} - U^N_{VN}$

$\mathbf{R_zT_z(R_xR_yT_y)}$	$\mathbf{R_zT_z(R_xT_y)}$
$U^{VN}_T - U^T_{VN}$, $U^{VN}_T - U^N_{VN}$, $U^{VN}_N - U^T_{VN}$, $U^{VN}_N - U^N_{VN}$	$U^{VN} - U^{VN}_T$, $U^{VN} - U^{VN}_N$, $U^{VN}_T - U^{VN}$, $U^{VN}_N - U^{VN}$

Table A.XVII. *Mobility properties of TNV-type PMs with 3-DoF with two parasitic mobility for* $\theta = 90^\circ$

$\mathbf{T_z(R_xR_yR_zT_xT_y)(R_xR_zT_xT_y)}$
$U^{VT} - U^T$, $U^{VT} - U^N$, $U^{VT} - U^{VN}$, $U^{VT} - U^T_N$, $U^{VT} - U^N_T$, $U^{VT} - U^{VN}_T$, $U^{VT} - U^{VN}_N$, $U^{VT} - U^{VN}_{VT}$, $U^{VT} - U^T_{VN}$, $U^{VT} - U^N_{VT}$, $U^{VT} - U^N_{VN}$, $U^{VT} - U^{VN}_{VT}$, $U^{VN} - U^{VT}$, $U^{VN} - U^T_{VT}$, $U^{VN} - U^N_{VT}$, $U^T_T - U^T_{VT}$, $U^T_T - U^N_{VT}$, $U^T_T - U^{VN}_{VT}$, $U^{VN}_T - U^{VT}$, $U^{VN}_T - U^T_{VT}$, $U^{VN}_T - U^N_{VT}$, $U^{VT}_T - U^T_{VT}$, $U^{VT}_T - U^N_{VT}$, $U^{VT}_T - U^{VN}_{VT}$, $U^{VN}_N - U^{VT}$, $U^{VN}_N - U^T_{VT}$, $U^{VN}_N - U^N_{VT}$, $U^{VT}_N - U^T_{VT}$, $U^{VT}_N - U^N_{VT}$, $U^{VT}_N - U^{VN}_{VT}$, $U^{VN}_{VT} - U^T$, $U^{VN}_{VT} - U^N$, $U^{VN}_{VT} - U^{VT}$, $U^{VN}_{VT} - U^T_N$, $U^{VN}_{VT} - U^N_T$, $U^{VN}_{VT} - U^T_T$, $U^{VN}_{VT} - U^N_N$, $U^{VN}_{VT} - U^T_{VT}$, $U^{VN}_{VT} - U^T_{VN}$, $U^{VN}_{VT} - U^N_{VT}$, $U^{VN}_{VT} - U^N_{VN}$, $U^{VN}_{VT} - U^{VT}_{VN}$

$\mathbf{T_z(R_xR_yR_zT_xT_y)(R_xR_zT_y)}$	$\mathbf{T_z(R_xR_yR_zT_xT_y)(R_yT_xT_y)}$
$U^{VT} - U^{VT}_{VN}$, $U^{VN} - U^{VT}_T$, $U^{VN} - U^{VT}_N$, $U^{VN} - U^{VT}_{VN}$, $U^{VN} - U^{VN}_{VT}$, $U^{VT}_T - U^{VN}$, $U^{VT}_T - U^{VN}_{VT}$, $U^{VT}_N - U^{VN}$, $U^{VN}_N - U^{VT}_{VN}$, $U^{VT}_{VN} - U^{VN}$, $U^{VN}_{VT} - U^{VN}_T$, $U^{VN}_{VT} - U^{VN}_N$, $U^{VN}_{VT} - U^{VT}_N$	$U^{VT}_T - U^T$, $U^{VT}_T - U^N$, $U^{VT}_T - U^T_N$, $U^{VT}_T - U^N_T$, $U^{VT}_T - U^{VN}_T$, $U^{VT}_T - U^{VN}_N$, $U^{VT}_T - U^{VN}_{VT}$

$\mathbf{T_z(R_xR_yR_zT_y)(R_zT_y)}$	$\mathbf{T_z(R_xR_yR_zT_y)(R_zT_y)}$
$U^{VT}_{VN} - U^T$, $U^{VT}_{VN} - U^N$, $U^{VT}_{VN} - U^T_N$, $U^{VT}_{VN} - U^N_T$, $U^{VT}_{VN} - U^T_{VN}$, $U^{VT}_{VN} - U^N_{VN}$	$U^{VT}_T - U^T_{VN}$, $U^{VT}_T - U^N_{VN}$, $U^{VT}_N - U^T_{VN}$, $U^{VT}_N - U^N_{VN}$

$\mathbf{T_z(R_xR_yT_xT_y)(R_yT_xT_y)}$
$U^{VN}_T - U^T$, $U^{VN}_T - U^N$, $U^{VN}_T - U^T_N$, $U^{VN}_T - U^N_T$, $U^{VN}_T - U^{VT}_T$, $U^{VN}_T - U^{VT}_N$, $U^{VT}_N - U^T$, $U^{VT}_N - U^N$, $U^{VT}_N - U^T_N$, $U^{VT}_N - U^N_T$, $U^{VT}_N - U^{VN}_T$, $U^{VT}_N - U^{VN}_N$, $U^{VN}_N - U^T$, $U^{VN}_N - U^N$, $U^{VN}_N - U^T_N$, $U^{VN}_N - U^N_T$, $U^{VN}_N - U^{VT}_T$, $U^{VN}_N - U^{VT}_N$

https://doi.org/10.1017/S0263574721001259 Published online by Cambridge University Press

Table A.XVII. *Continued*

$\mathbf{T_z(R_xR_zT_y)(R_yT_x)}$	$\mathbf{T_z(R_xR_zT_y)(R_zT_y)}$
$U^{VT} - U_T^{VT}$, $U^{VT} - U_N^{VT}$, $U_T^{VT} - U^{VT}$, $U_T^{VN} - U_{VT}^{VN}$, $U_N^{VT} - U^{VT}$, $U_N^{VT} - U^{VT}$, $U_N^{VN} - U_{VT}^{VN}$, $U_{VT}^{VN} - U_T^{VN}$, $U_{VT}^{VN} - U_N^{VN}$, $U_{VN}^{VT} - U_{VT}^{VN}$	$U_T^{VT} - U_{VN}^{VT}$, $U_N^{VT} - U_{VN}^{VT}$, $U_{VN}^{VT} - U_T^{VT}$, $U_{VN}^{VT} - U_N^{VT}$, $U_{VN}^{VT} - U_{VN}^{VT}$
$\mathbf{T_z(R_xT_y)(R_yT_x)}$	$\mathbf{T_z(R_yT_x)(R_xT_y)}$
$U_T^{VT} - U_T^{VT}$, $U_T^{VT} - U_N^{VT}$, $U_T^{VN} - U_T^{VN}$, $U_T^{VN} - U_N^{VN}$, $U_N^{VT} - U_T^{VT}$, $U_N^{VT} - U_N^{VT}$, $U_N^{VN} - U_T^{VN}$, $U_T^{VN} - U_N^{VN}$	$U^{VT} - U^{VT}$

Table A.XVIII. *Mobility properties of XYV-type PMs with 5-DoF*

$\mathbf{R_xR_yT_xT_yT_z}$
$U^X - U^X$, $U^X - U^Y$, $U^X - U_Y^X$, $U^X - U_X^Y$, $U^Y - U^X$, $U^Y - U^Y$, $U^Y - U_Y^X$, $U^Y - U_X^Y$, $U_Y^X - U^X$, $U_Y^X - U^Y$, $U_Y^X - U_Y^X$, $U_Y^X - U_X^Y$, $U_X^Y - U^X$, $U_X^Y - U^Y$, $U_X^Y - U_Y^X$, $U_X^Y - U_X^Y$

Table A.XIX. *Mobility properties of XYV-type PMs with 4-DoF*

$\mathbf{R_xR_yT_xT_z}$
$U^X - U^{VY}$, $U^X - U_X^{VY}$, $U^X - U_{VY}^X$, $U^X - U_{VY}^Y$, $U^X - U_Y^{VY}$, $U^Y - U^{VY}$, $U^Y - U_X^{VY}$, $U^Y - U_{VY}^X$, $U^Y - U_{VY}^Y$, $U^Y - U_Y^{VY}$, $U_Y^X - U^{VY}$, $U_Y^X - U_X^{VY}$, $U_Y^X - U_{VY}^X$, $U_Y^X - U_{VY}^Y$, $U_Y^X - U_Y^{VY}$, $U_Y^X - U^{VY}$, $U_X^Y - U_X^{VY}$, $U_X^Y - U_{VY}^X$, $U_X^Y - U_{VY}^Y$, $U_X^Y - U_Y^{VY}$
$\mathbf{R_xR_yT_yT_z}$
$U^X - U^{VX}$, $U^X - U_X^{VX}$, $U^X - U_{VX}^X$, $U^X - U_{VX}^Y$, $U^X - U_Y^{VX}$, $U^Y - U^{VX}$, $U^Y - U_X^{VX}$, $U^Y - U_{VX}^X$, $U^Y - U_{VX}^Y$, $U^Y - U_Y^{VX}$, $U_Y^X - U^{VX}$, $U_Y^X - U_X^{VX}$, $U_Y^X - U_{VX}^X$, $U_Y^X - U_{VX}^Y$, $U_Y^X - U_Y^{VX}$, $U_Y^X - U^{VX}$, $U_X^Y - U_X^{VX}$, $U_X^Y - U_{VX}^X$, $U_X^Y - U_{VX}^Y$, $U_X^Y - U_Y^{VX}$

Table A.XX. *Mobility properties of XYV-type PMs with 4-DoF with one parasitic mobility*

$\mathbf{R_xR_yT_z(R_zT_y)}$
$U^X - U_{VX}^{VY}$, $U^Y - U_{VX}^{VY}$, $U_Y^X - U_{VX}^{VY}$, $U_X^Y - U_{VX}^{VY}$
$\mathbf{R_xT_yT_z(R_yT_x)}$
$U^{VX} - U^{VX}$, $U_X^{VX} - U_X^{VX}$, $U_X^{VX} - U_Y^{VX}$, $U_{VX}^X - U^X$, $U_{VX}^X - U^Y$, $U_{VX}^X - U_Y^X$, $U_{VX}^X - U_X^Y$, $U_{VX}^X - U_{VX}^Y$, $U_{VX}^X - U_{VX}^X$, $U_{VX}^Y - U^X$, $U_{VX}^Y - U^Y$, $U_{VX}^Y - U_Y^X$, $U_{VX}^Y - U_X^Y$, $U_{VX}^Y - U_{VX}^X$, $U_{VX}^Y - U_{VX}^Y$, $U_Y^{VX} - U_X^{VX}$, $U_Y^{VX} - U_Y^{VX}$

https://doi.org/10.1017/S0263574721001259 Published online by Cambridge University Press

Table A.XX. *Continued*

$\mathbf{R_yT_xT_z(R_xT_y)}$
$U^{VY}-U^{VY}$, $U_X^{VY}-U_X^{VY}$, $U_X^{VY}-U_Y^{VY}$, $U_{VY}^{X}-U^{X}$, $U_{VY}^{X}-U^{Y}$, $U_{VY}^{X}-U_Y^{X}$, $U_{VY}^{X}-U_X^{Y}$, $U_{VY}^{X}-U_{VY}^{X}$, $U_{VY}^{X}-U_{VY}^{Y}$, $U_{VY}^{Y}-U^{X}$, $U_{VY}^{Y}-U^{Y}$, $U_{VY}^{Y}-U_X^{X}$, $U_{VY}^{Y}-U_X^{Y}$, $U_{VY}^{Y}-U_{VY}^{X}$, $U_{VY}^{Y}-U_{VY}^{Y}$, $U_Y^{VY}-U_X^{VY}$, $U_Y^{VY}-U_Y^{VY}$
$\mathbf{R_yT_xT_z(R_xR_zT_y)}$
$U^{VY}-U_X^{VY}$, $U^{VY}-U_Y^{VY}$, $U_X^{VY}-U^{VY}$, $U_{VY}^{X}-U^{VY}$, $U_{VY}^{X}-U_X^{VY}$, $U_{VY}^{X}-U_Y^{VY}$, $U_{VY}^{Y}-U^{VY}$, $U_{VY}^{Y}-U_X^{VY}$, $U_{VY}^{Y}-U_Y^{VY}$, $U_Y^{VY}-U^{VY}$

Table A.XXI. *Mobility properties of XYV-type PMs with 4-DoF with two parasitic mobility*

$\mathbf{R_xT_z(R_yR_zT_xT_y)(R_zT_xT_y)}$	$\mathbf{R_xT_z(R_yT_x)(R_zT_y)}$
$U_{VX}^{X}-U^{VY}$, $U_{VX}^{Y}-U^{VY}$	$U_{VX}^{X}-U_Y^{VY}$, $U_{VX}^{X}-U_{VY}^{Y}$, $U_{VX}^{X}-U_Y^{VY}$, $U_{VX}^{X}-U_{VX}^{VY}$, $U_{VX}^{Y}-U_X^{VY}$, $U_{VX}^{Y}-U_Y^{VY}$, $U_{VX}^{Y}-U_{VX}^{VY}$
$\mathbf{R_xT_z(R_yT_xT_y)(R_yT_xT_y)}$	$\mathbf{R_yT_z(R_xR_zT_xT_y)(R_zT_xT_y)}$
$U_{VX}^{X}-U_{VY}^{X}$, $U_{VX}^{Y}-U_{VY}^{X}$, $U_{VX}^{Y}-U_{VY}^{Y}$	$U^{VY}-U_{VX}^{VY}$, $U_{VY}^{X}-U_{VX}^{VY}$, $U_{VY}^{Y}-U_{VX}^{VY}$
$\mathbf{R_yT_z(R_xR_zT_y)(R_zT_y)}$	
$U_X^{VY}-U_{VX}^{VY}$, $U_{VY}^{X}-U_{VX}^{X}$, $U_{VY}^{X}-U_{VX}^{Y}$, $U_{VY}^{Y}-U_{VX}^{X}$, $U_{VY}^{Y}-U_{VX}^{Y}$, $U_Y^{VY}-U_{VX}^{VY}$	

Table A.XXII. *Mobility properties of XYV-type PMs with 4-DoF with three parasitic mobility*

$\mathbf{T_z(R_xR_yR_zT_xT_y)(R_yR_zT_xT_y)(R_zT_xT_y)}$	$\mathbf{T_z(R_xR_zT_y)(R_yT_x)(R_zT_y)}$
$U_{VX}^{VY}-U^{VY}$	$U_{VX}^{VY}-U_X^{VY}$, $U_{VX}^{VY}-U_Y^{VY}$, $U_{VY}^{VX}-U_{VY}^{VX}$

Table A.XXIII. *Mobility properties of XYV-type PMs with 3-DoF*

$\mathbf{R_xR_yT_z}$
$U^{X}-U_{VY}^{VX}$, $U^{Y}-U_{VY}^{VX}$, $U_Y^{X}-U_{VY}^{VX}$, $U_X^{Y}-U_{VY}^{VX}$
$\mathbf{R_xT_yT_z}$
$U^{VX}-U^{X}$, $U^{VX}-U^{Y}$, $U^{VX}-U_Y^{X}$, $U^{VX}-U_X^{Y}$, $U^{VX}-U_X^{VX}$, $U^{VX}-U_{VX}^{X}$, $U^{VX}-U_{VX}^{Y}$, $U^{VX}-U_Y^{VX}$, $U_X^{VX}-U^{X}$, $U_X^{VX}-U^{Y}$, $U_X^{VX}-U^{VX}$, $U_X^{VX}-U_Y^{X}$, $U_X^{VX}-U_X^{Y}$, $U_X^{VX}-U_{VX}^{X}$, $U_X^{VX}-U_{VX}^{Y}$, $U_{VX}^{X}-U^{VX}$, $U_{VX}^{X}-U_X^{VX}$, $U_{VX}^{X}-U_Y^{VX}$, $U_{VX}^{Y}-U^{VX}$, $U_{VX}^{Y}-U_X^{VX}$, $U_{VX}^{Y}-U_Y^{VX}$, $U_Y^{VX}-U^{X}$, $U_Y^{VX}-U^{Y}$, $U_Y^{VX}-U^{VX}$, $U_Y^{VX}-U_Y^{X}$, $U_Y^{VX}-U_X^{Y}$, $U_Y^{VX}-U_{VX}^{X}$, $U_Y^{VX}-U_{VX}^{Y}$,
$\mathbf{R_yT_xT_z}$
$U^{VY}-U^{X}$, $U^{VY}-U^{Y}$, $U^{VY}-U_Y^{X}$, $U^{VY}-U_X^{Y}$, $U^{VY}-U_X^{VY}$, $U^{VY}-U_{VY}^{Y}$, $U_X^{VY}-U^{X}$, $U_X^{VY}-U^{Y}$, $U_X^{VY}-U_Y^{X}$, $U_X^{VY}-U_X^{Y}$, $U_X^{VY}-U_{VY}^{X}$, $U_X^{VY}-U_{VY}^{Y}$, $U_Y^{VY}-U^{X}$, $U_Y^{VY}-U^{Y}$, $U_Y^{VY}-U_X^{X}$, $U_Y^{VY}-U_X^{Y}$, $U_Y^{VY}-U_{VY}^{X}$, $U_Y^{VY}-U_{VY}^{Y}$

https://doi.org/10.1017/S0263574721001259 Published online by Cambridge University Press

Table A.XXIV. *Mobility properties of XYV-type PMs with 3-DoF with one parasitic mobility*

$\mathbf{R_xT_z(T_xT_y)}$
$U^{VX} - U^{VY}$, $U_X^{VX} - U_X^{VY}$, $U_X^{VX} - U_Y^{VY}$, $U_Y^{VX} - U_X^{VY}$, $U_Y^{VX} - U_Y^{VY}$

$\mathbf{R_xT_z(R_yR_zT_xT_y)}$
$U^{VX} - U_X^{VY}$, $U^{VX} - U_{VY}^{X}$, $U^{VX} - U_Y^{VY}$, $U^{VX} - U_{VX}^{VY}$, $U_X^{VX} - U^{VY}$, $U_X^{VX} - U_{VY}^{X}$, $U_X^{VX} - U_{VY}^{Y}$, $U_Y^{VX} - U^{VY}$, $U_Y^{VX} - U_{VY}^{X}$, $U_Y^{VX} - U_{VY}^{Y}$

$\mathbf{R_xT_z(R_yT_xT_y)}$	$\mathbf{R_xT_z(R_yT_x)}$	$\mathbf{R_xT_z(R_yR_zT_y)}$	$\mathbf{R_xT_z(R_yT_y)}$
$U^{VX} - U_{VY}^{VX}$	$U_X^{VX} - U_{VY}^{VX}$, $U_Y^{VX} - U_{VY}^{VX}$	$U_X^{VX} - U_{VX}^{VY}$, $U_Y^{VX} - U_{VX}^{VY}$	$U_{VX}^{X} - U_{VY}^{VX}$, $U_{VX}^{Y} - U_{VY}^{VX}$

$\mathbf{R_yT_z(TxTy)}$	$\mathbf{R_yT_z(R_xR_zT_xT_y)}$
$U^{VY} - U^{VX}$, $U_X^{VY} - U_X^{VX}$, $U_X^{VY} - U_Y^{VX}$, $U_Y^{VY} - U_X^{VX}$, $U_Y^{VY} - U_Y^{VX}$	$U^{VY} - U_X^{VX}$, $U^{VY} - U_Y^{VX}$, $U^{VY} - U_{VY}^{VX}$, $U_X^{VY} - U_{VY}^{VX}$, $U_Y^{VY} - U_{VY}^{VX}$

$\mathbf{R_yT_z(R_zT_xT_y)}$	$\mathbf{R_yT_z(R_xR_zT_y)}$	$\mathbf{R_yT_z(R_zT_y)}$
$U^{VY} - U_{VX}^{X}$, $U^{VY} - U_{VX}^{Y}$,	$U_X^{VY} - U^{VX}$, $U_Y^{VY} - U^{VX}$,	$U_X^{VY} - U_{VX}^{X}$, $U_X^{VY} - U_{VX}^{Y}$, $U_Y^{VY} - U_{VX}^{X}$, $U_Y^{VY} - U_{VX}^{Y}$

$\mathbf{R_yT_z(R_xT_y)}$
$U_{VY}^{X} - U^{VX}$, $U_{VY}^{X} - U_X^{VX}$, $U_{VY}^{X} - U_Y^{VX}$, $U_{VY}^{X} - U_{VY}^{VX}$, $U_{VY}^{Y} - U^{VX}$, $U_{VY}^{Y} - U_Y^{VX}$, $U_{VY}^{Y} - U_Y^{VX}$ $U_{VY}^{Y} - U_{VY}^{VX}$

Table A.XXV. *Mobility properties of XYV-type PMs with 3-DoF with two parasitic mobility*

$\mathbf{T_z(R_xR_yR_zT_xT_y)(R_xR_zT_xT_y)}$	$\mathbf{T_z(R_xR_yR_zT_xT_y)(R_xR_zT_y)}$
$U_{VX}^{VY} - U_{VY}^{VX}$	$U_{VX}^{VY} - U^{VX}$, $U_{VX}^{VY} - U_X^{VX}$, $U_{VX}^{VY} - U_Y^{VX}$

$\mathbf{T_z(R_xR_yR_zT_xT_y)(R_yR_zT_xT_y)}$
$U_{VY}^{VX} - U^{X}$, $U_{VY}^{VX} - U^{Y}$, $U_{VY}^{VX} - U^{VY}$, $U_{VY}^{VX} - U_Y^{X}$, $U_{VY}^{VX} - U_X^{Y}$, $U_{VY}^{VX} - U_X^{VY}$, $U_{VY}^{VX} - U_{VX}^{X}$, $U_{VY}^{VX} - U_{VY}^{X}$, $U_{VY}^{VX} - U_{VX}^{Y}$, $U_{VY}^{VX} - U_{VY}^{Y}$, $U_{VY}^{VX} - U_Y^{VY}$, $U_{VY}^{VX} - U_{VX}^{VY}$

$\mathbf{T_z(R_xR_yT_xT_y)(R_yT_xT_y)}$	$\mathbf{T_z(R_xT_y)(R_yT_x)}$	$\mathbf{T_z(R_yR_zT_xT_y)(R_zT_xT_y)}$
$U_{VY}^{VX} - U^{VX}$	$U_{VY}^{VX} - U_X^{VX}$, $U_{VY}^{VX} - U_Y^{VX}$, $U_{VY}^{VX} - U_{VY}^{VX}$	$U_{VX}^{VY} - U_{VY}^{X}$, $U_{VX}^{VY} - U_{VY}^{Y}$

$\mathbf{T_z(R_yT_x)(R_zT_y)}$
$U_{VX}^{VY} - U^{X}$, $U_{VX}^{VY} - U^{Y}$, $U_{VX}^{VY} - U_Y^{X}$, $U_{VX}^{VY} - U_X^{Y}$, $U_{VX}^{VY} - U_X^{VY}$, $U_{VX}^{VY} - U_{VX}^{X}$, $U_{VX}^{VY} - U_{VX}^{Y}$

Cite this article: S. Boztaş and G. Kiper (2022). "Enumeration and instantaneous mobility analysis of a class of 3-UPU parallel manipulators with equilateral triangular platforms", Robotica **40**, 1538–1569. https://doi.org/10.1017/S0263574721001259
https://doi.org/10.1017/S0263574721001259 Published online by Cambridge University Press